Spring 5-2016

Lesion identification and the effect of lesion on motor mapping after stroke

Ruixi Zhou
Washington University in St. Louis

WASHINGTON UNIVERSITY IN ST. LOUIS

School of Engineering and Applied Science

Department of Biomedical Engineering

Thesis Examination Committee:
Maurizio Corbetta, Chair
Dennis Barbour
Dan Moran

Lesion identification and the effect of lesion on motor mapping after stroke

by

Ruixi Zhou

A thesis presented to the School of Engineering
of Washington University in St. Louis in partial fulfillment of the
requirements for the degree of
Master of Science

May 2016

Saint Louis, Missouri

Contents

List of Figures

List of Tables

Acknowledgments

I would like to express my sincere gratitude to my supervisor Dr. Maurizio Corbetta, for providing me the honor to join in his lab. His expertise, patience, understanding and motivation guided me to make this thesis possible.

Except for my advisor, I would like to thank the rest of my committee members: Prof. Dennis Barbour and Prof. Dan Moran, for their insightful comments and great help to my thesis.

I also would like to thank the wonderful people in the Corbetta lab: Prof. Gordon Shulman, Tomer Livne, Joshua S. Siegel, Serguei Astafiev, Hong Xin, Nicholas Metcalf and Dohyun Kim, for their stimulating ideas and generous encouragement.

Special thanks goes to Lenny Ramsey, who has always been mentoring me since my participation in the lab. Without her initial ideas and generous help from the beginning to the end, I cannot finish this thesis.

Ruixi Zhou

Washington University in St. Louis
May 2016

Dedicated to my parents, Kai Zhou and Jianping Zeng,
for their love and support throughout my life

ABSTRACT OF THE THESIS

Lesion identification and investigation of its effect

on motor mapping after stroke

by

Ruixi Zhou

Master of Science in Biomedical Engineering

Washington University in St. Louis, 2016

Research Advisor: Professor Maurizio Corbetta

Stroke is the most common cause of long-term severe disability and the motor system that is most commonly affected in stroke. One of the mechanisms that underlies recovery of motor deficits is reorganization or remapping of functional representations around the motor cortex. This mechanism has been shown in monkeys, but results in human subjects have been variable. In this thesis, I used a database that includes longitudinal behavioral and multimodal imaging data in both stroke patients and healthy controls for two research projects. Firstly, I improved an automatic lesion segmentation method to aid in the identification of the location and extent of the stroke in structural magnetic resonance imaging (MRI) images. I developed a point and click interface that allows for the automatic segmentation as well as selecting lesions generated at different thresholds based on the contrast of the T1 images. Second, I investigated the effect of subcortical strokes on motor representations by measuring changes in the topography of inter-hemispheric resting state functional connectivity (FC) MRI to track changes of the hand representation in the damaged hemisphere shows a higher variation across the medial-lateral axis, suggesting a shift in neighboring body representations along the motor strip. During recovery, however, there is a shift in an anterior-

posterior direction suggesting a shift into sensory and premotor regions. Obtaining lesion profile and understanding its effect on the functional connectivity can provide us with useful information on the effects of stroke on brain structure and function, which in turn will help in the prognosis and rehabilitation of stroke patients.

Preface

Stroke occurs when blood flow to an area of the brain is interrupted by a clot (ischemia) or a blood vessel rupture (hemorrhage). Lack of blood flow leads to lack of oxygen, which in turn leads to neuronal dysfunction and death. Stroke is the second leading causes of death for people over 60 years old and the fifth leading cause of death in people aged 15 to 59 (World Heart Federation, Geneva, Switzerland). The brain controls and processes all of our inputs and outputs such as pictures, sounds, feeling, movement and speech. Stroke can cause focal lesions in the brain of different sizes and at different locations, which can result in different kinds of neurologic deficits. One of the neural systems that is affected most commonly is the motor system, leading to both short-term and long-term disabilities of controlling movement. At acute stage more than two-thirds of patients show motor deficit including (hemi-) paresis or loss of dexterity (Kwan et al. 1999).

Lesion size and the location of damage can also help in prediction (C. L. Chen et al. 2000). Magnetic resonance imaging (MRI) takes advantage of the magnetic property of certain atomic nuclei, e.g. the hydrogen nucleus present in water molecules. The hydrogen nuclei will partially align under a magnetic field and subsequently return to equilibrium to emit a radio signal. Since different tissues in the brain contain various molecules, the different nuclear mobility, molecular structure and other factors (Hanson 2008) make it possible to capture differences between normal and abnormal tissues when identifying the damage caused by stroke. Physicians can take advantage of the information from these images, such as lesion size, location, and contrast as important criteria for diagnosis and prognosis of outcome post-stroke. Before the use of computers in radiology, radiologists could only visually identify lesions on physical films. With the introducing of digital scans and increased computer power, people can segment lesions on the computer. Currently, however, the work of lesion identification still requires manual tracing by trained professionals. This process not only takes a lot of time and effort particularly for high-resolution images, but the results are somewhat subjective, which leads to variations in the definition of lesion borders. Therefore, an automatic segmentation method that can relieve people from this laborious work and has a more objective standard is of great importance for both clinical use and research purposes. One goal of my thesis is therefore to improve on an automatic segmentation method for the localization of abnormal tissue in stroke.

Structural damage to the brain results in changes of brain function. One of the mechanisms of recovery is an increase in neuroplasticity in the regions around the stroke. Plasticity refers to a series of mechanisms (genetic, molecular, cellular, systems) that are activated by injury and that can lead to adaptation and reorganization of function (Elbert and Rockstroh 2004; Pascual-Leone et al. 2005). After acute injury, in the first few weeks and months post-stroke, recovery from motor deficits is thought to be driven by neural reorganization (Murphy and Corbett 2009). Neural reorganization includes a variety of mechanisms including angiogenesis, glial and neuro genesis, synaptic sprouting, and physiological rebalancing of existing connections (Wieloch and Nikolich 2006; Carmichael 2006). A mechanism that has been clearly demonstrated in animal studies is the re-mapping of cortical representation in motor cortex after stroke causing motor deficits (R J Nudo and Milliken 1996; Dijkhuizen et al. 2001). Specifically, after stroke neurons responsive to different body parts can respond to movements previously controlled by the injured motor neurons.

In humans it has been suggested that the initial degree of functional disorganization and the following dynamic reorganization can determine the amount of the acute impairment and the level of post-stroke recovery, respectively (Carter, Shulman, and Corbetta 2012). Yet, while task activation functional MRI (fMRI) studies have provided important information about correlations between damage and recovery, it is not clear how these results match the animal literature on cortical remapping (Randolph J. Nudo 2006). Task activations, both location and magnitude, can be biased due to differences in the abilities of patients to be able to perform the task. Fro example, the amplitude of a movement in a motor task influences the magnitude of blood oxygenation level-dependent (BOLD) signal that we measured (Waldvogel et al. 1999). Moreover, the task fMRI methods just highlights the peak activation without provide information about a shift in the whole motor representation (e.g. from hand to leg), which is the hallmark of the animal studies.

Therefore in this study, I elected to measure changes in motor map organization using a different method, namely resting state fMRI, which only require the subject to lie in the scanner quietly without thinking. Comparing with the relatively small change (i.e. ~1% of BOLD response over baseline at 3T scanner) of neuronal activity driven by task, the fluctuation of fMRI signal at resting state are larger (5-20%). Thus we can map the alteration of temporal correlation between areas at the

level of single subjects. Because of the corresponding somatotopic organization of left and right primary motor cortex (Van Den Heuvel and Pol 2010), I decided to measure the functional connectivity between left and right pre-central and post-central cortex, which contains primary motor, sensory, and premotor cortex looking for changes in the location and strength of the inter-hemispheric connectivity in the hand representation. Since hand deficits are the most common post-stroke, this strategy could be helpful to map reorganization of motor cortical maps in stroke.

In summary, both structural and functional information can help us in better understanding the mechanisms underlying acute change and the recovery process. Understanding both structural and functional effects of stroke will be therefore of great importance for improving current rehabilitative, pharmacological, and stimulation treatment strategies for stroke. In my thesis project I develop two methods for looking at the structural and functional effects of stroke on brain function.

Chapter 1

Automatic segmentation

1.1 Background

1.1.1 Existing methods

Over the past few decades, multiple methods for the semi-automatic and automatic lesion identification have emerged as the manual identification is subjective and time consuming. The current options can be categorized into two groups: unsupervised and supervised learning methods (García-Lorenzo et al. 2013). Unsupervised methods are primarily cluster-based approaches, separating voxels into separate categories of normal and abnormal tissue, sometimes combined with general anatomical information about grey and white matter distributions (Wang et al. 2014; Birgani, Ashtiyani, and Asadi 2008; Pham and Prince 1999). These methods are fit for studies with smaller numbers of patients as there is no need for a manually segmented sample for training the model. However, without taking the lesion information into consideration, the sensitivity of these methods is lower than that of supervised methods. Supervised learning methods "learn" from previous information about lesions, which is usually obtained by manual segmentation. This prior lesion information from a "learning group" (subjects that have already been segmented) is used to build a model of lesions. This model is subsequently employed to detect the lesions in target subjects. Machine learning based lesion identification, such as using support vector machine (SVM(Maier et al. 2014; Lao et al. 2008)), extra tree forest (Maier et al. 2015) or k-nearest neighbors (k-NN) (Anbeek et al. 2004) are examples of supervised learning methods. In order to ensure that the learning process is correct and unbiased, supervised methods require a large database to "learn". The establishment of such a large lesion database takes a lot of time and effort, as lesions need to be

manually traced before the automatic segmentation. Most unsupervised and unsupervised methods are based on intensity information only, but others have used other information obtained from images as other criteria to segment lesions (Feng, Tierney, and Magnotta 2012; Ozenne et al. 2014; Schmidt et al. 2005; Tu et al. 2005). One method is to use spatial information. Instead of taking advantage of just the one intensity of a single voxel, the intensities of the surrounding voxels are also taken into account. In addition there are studies aiming to use multi-channel images to extract various features from different types of images (such as T1-weighted images, T2-weighted images, fluid attenuation inversion recovery (FLAIR) images and diffusion weighted imaging (DWI)), and combining the information to identify the lesion (Lao et al. 2008; Misaki et al. 2015; Shi et al. 2013).

In summary, supervised learning methods require time and effort to build a database with prior lesion information, but they are more accurate. In contrast, unsupervised learning methods only need the target image to identify lesion. Considering the great variability for stroke patients' brain images, it can be hard to extract accurate lesion based on one image. Thus, an efficient and accurate lesion identification method that does not require prior lesion information has still not been developed.

1.1.2 Hypothesis

Considering the large variance of stroke lesions we do not think that it is feasible to build a complete lesion model from our database. We hypothesize that after accurate spatial registration of both healthy subjects and stroke patients, an unsupervised method, just using distributions of the grey matter (GM) and white matter (WM) of a group of healthy controls can be used for detection of outliers to identify the lesions in MRI images. Then, to decrease false positives we propose adding a clustering algorithm. This method does not require a large group of predefined lesions for training, but we can use the previously manually segmented lesion of a large cohort of stroke patients to test the accuracy of our automatic segmentation sequence.

1.2 Method

MRI images such as T1-weighted or T2-weighted images have been widely used for structural segmentation and pathology recognition in the brain because of their high sensitivities for different kinds of tissues. Here, we developed a pipeline, which is compatible for both modalities to automatically identify lesions based on the Automatic Lesion Identification toolbox (ALI) created by Seghier and colleagues (Seghier et al. 2008). This package is embedded in SPM12 software (Wellcome Trust Centre for Neuroimaging, London, UK, http://www.fil.ion.ucl.ac.uk/spm/) and it uses a multi-step approach to segment the lesions. The ALI toolbox has a linear spatial registration (Talairach and Tournoux 1988) implemented yet we chose to add a non-linear transformation to register the brain images of healthy subjects and stroke subjects for a more robust alignment which should also lead to improved accuracy of lesion detection. After obtaining the initial lesion result from ALI toolbox, we then added a smart clustering algorithm to greatly increase the true positives and decrease the false negatives. A schematic of the method is shown in Figure 1.1.

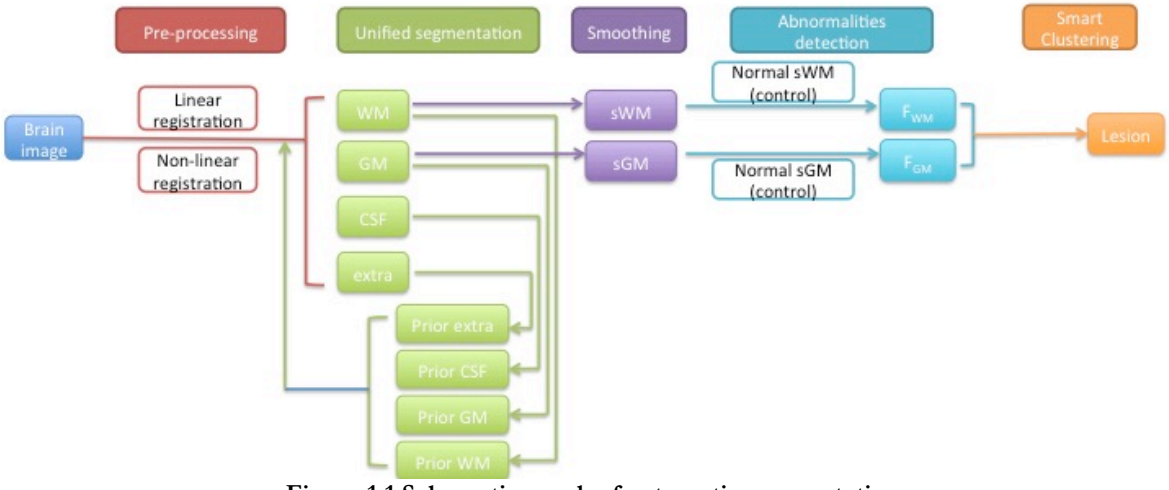

Figure 1.1 Schematic graph of automatic segmentation

1.2.1 Data acquisition

A database (Corbetta et al. 2015) containing the MRI images of 132 stroke patients was used. The stroke patients were recruited from the stroke service at Barnes-Jewish Hospital (BJH), with the help of the Washington University Cognitive Rehabilitation Research Group (CRRG)(Dr. Lisa Connor) from 5/1/2008 to 5/30/2013. Data was collected in the stroke subjects at 3 time points (acute: 2 weeks after stroke, chronic1: 3 months after stroke, chronic2: 1 year after stroke) and included MRI scans (T1, T2, and FLAIR), resting state functional MRI and a large battery of behavioral measures. A healthy subject group (N = 45) is use as controls on whom the same data was collected at two time points 3 months apart. The subjects in the healthy control group are matched with the study sample for age, gender and years of education.

Scanning was performed using Siemens 3T Tim-Trio scanner and the standard 12-channel head coil at the Washington University School of Medicine. The two structural scans include a sagittal MP-RAGE T1-weighted image (TR=1950 msec, TE=2.26 msec, flip angle=9 degree, voxel size=1.0×1.0×1.0 mm, slice thickness=1.00 mm) and a transverse turbo spin-echo T2-weighted image (TR=2500 msec, TE=435 msec, voxel size=1.0×1.0×1.0 mm, slice thickness=1.00 mm) (Corbetta et al. 2015).

1.2.2 Preprocessing

T2-weighted images are registered to T1-weighted images using a cross-modal process based on the alignment of image intensity gradient (Rowland et al. 2005). Then the images are transformed into atlas-space (Talairach and Tournoux 1988) through a 12-parameter affine transformation, linearly registering the whole brain to a similar size, shape and orientation. Linear registration can only rotate, zoom and shear one image to match a common space by linear deformation. This allows for the whole size of brain match with each other in the images, some local areas such as sulci and gyri within the brain vary. To make the brain images more consistent, a non-linear registration is performed through FSL (Analysis Group, FMRIB, Oxford, UK, http://fsl.fmrib.ox.ac.uk/fsl/fslwiki/) to permit local deformations. Since some stroke patients have enlarged ventricles and which is quite unusual in healthy subject, directly comparing the images of

the above two will result in identifying the abnormal ventricle as lesion. Nonlinear registration is thus used to remove the influence of abnormal tissues that are not lesions. SPM was used to mask out areas outside of the brain in the aligned image, and to smooth and apply bias correction (Ashburner and Friston 2005) to reduce the effect of intensity inhomogeneity caused by MRI settings and the patients' position.

1.2.3 Unified segmentation

The ALI toolbox (Seghier et al. 2008) in SPM12 was used for the segmentation of the lesions. The first step is to separate the voxels into white matter (WM), grey matter (GM) and cerebrospinal fluid (CSF). This step combined with bias correction is implemented using the commands in ALI toolbox to generate a probabilistic modal, which is used for subject-specific classification in SPM (for more details see Ashburner and Friston 2005). The brain images of healthy subjects are segmented into the above three groups based on the prior intensity information of WM, GM and CSF from predefined priors, which were previously created as templates based on 452 healthy controls (International Consortium for Brain Mapping, http://www.loni.ucla.edu/ICBM/). Each prior defines the probability of a voxel belonging to a category. The voxels is assigned to the category with which it has the highest likelihood, which is based on the intensity and the probability. However, abnormal tissues (eg. lesions) cannot reliably classify into one of the three categories. For example, a lesion in a T1-weighted image can have the intensity of grey matter where normally white matter exists, causing a mismatch between spatial and intensity information. Therefore, voxels that have a low probability in the three categories are put in a fourth group. Since the usually misclassified voxels often appear within WM, the ALI toolbox calculates the general extra group criteria for first use based on the prior intensity information of WM and CSF:

$$\boldsymbol{G_{extra} = \frac{G_{WM}+G_{CSF}}{2}} \quad (1.1)$$

Where G_{WM} and G_{CSF} are standard probabilities of WM and CSF in normal brain. Using equation 1.1 as a prior to define the extra group, this fourth group consists of subject specific abnormal voxels. Subsequently, the procedure of classifying the brain into different groups is implemented again,

including this newly formed extra group (after a refinement that removes the extra group voxels with a probability below one third) as a prior to increase the accuracy of classification, especially for the lesion voxels whose intensity is in the range of WM and GM (Seghier et al. 2008). After this second iteration, the resulting WM and GM maps are smoothed using a Gaussian kernel of 8mm full-width-at-half-maximum (FWHM), to create separate image files of WM and GM for the use in the next step in which the lesion is identified. This process is performed on each of our patients and controls.

1.2.4 Abnormalities detection

In MRI images the image contrast is a function of tissue density, measuring the proton density. In T1-weighted images, the intensities of one type tissue are consistent because of their similar constitution while tissues with higher fat content such as white matter are brighter than grey matter tissue (Koenig et al. 1990). The difference of intensities in image caused by the above property can be used to detect of abnormal tissues in the brain through Fuzzy Clustering with fixed Prototypes (FCP) (for more details, see (Seghier, Friston, and Price 2007)). This time we are using our own age matched healthy subjects to compare the patients. Using the maps created in the previous step, fuzzy sets representing the probability WM and GM are formed containing WM and GM of all control subjects as well as the target patient. First, to identify the white matter abnormal tissue of the patient, the intensity of voxel n ($n = 1,2,\ldots,N_{voxel}$) in WM for one subject (the patient or a control subject) j ($j = 1,2,\ldots, N_{sub}$) in the fuzzy set is compared with the mean value of voxel n in the WM fuzzy set. A similarity metric S_{nj} is used to quantify the difference for voxel n in subject j:

$$\boldsymbol{S_{nj} = 1 - \tanh\left(\frac{N_{sub}}{N_{sub}-1} \times \frac{X_{nj} - \overline{X_n}}{\alpha}\right)} \quad (1.2)$$

Where $\boldsymbol{\alpha}$ is a constant "tuning" parameter and tanh is the hyperbolic tangent. $\boldsymbol{X_{nj}}$ is the value of j-th subject at voxel n and $\boldsymbol{\overline{X_n}}$ is the mean value of voxel n over all subjects in the fuzzy set. Furthermore, this similarity metric S_{nj} is used to quantify the degree of membership M_{nj} of voxel n to class j:

$$\boldsymbol{M_{nj}} = \frac{\boldsymbol{S_{nj}^{\lambda}}}{\sum_j \boldsymbol{S_{nj}^{\lambda}}} \qquad (1.3)$$

Where $\boldsymbol{\lambda}$ is another tuning parameter. Subsequently, when *j* indexes the patient and the value of M_{nj} is lower than threshold T, the *n*-th voxel is defined as a part of the lesion set F_{WM}, which contains the voxels that have a low probability in WM (even though it is spatially within WM) for this patient. The same procedure is repeated to get the fuzzy set F_{GM} for the grey matter. Finally, the two sets F_{WM} and F_{GM} are unified and voxels that have a low probability for either WM or GM are identified as abnormal.

1.2.5 Post-processing: clustering

Using this method we obtained the initial lesion results by extracting the abnormal tissue. However, the human brain is highly variable even in healthy subjects the consistently appearing gyri and sulci exhibit pronounced variability in size and configuration (Thompson et al. 1996), thus this method resulted in a high number of false positives. Using a default threshold (T = 0.3) of fuzzy degree of membership *M* (*M*= [0,1]) to decide whether the voxel is part of the lesion gave highly varied results. Figure 1.2 shows the result using a default threshold, which in this case leads to incomplete lesion identification. Figure 1.3 (a) shows a case where the lower threshold leads to false positives.

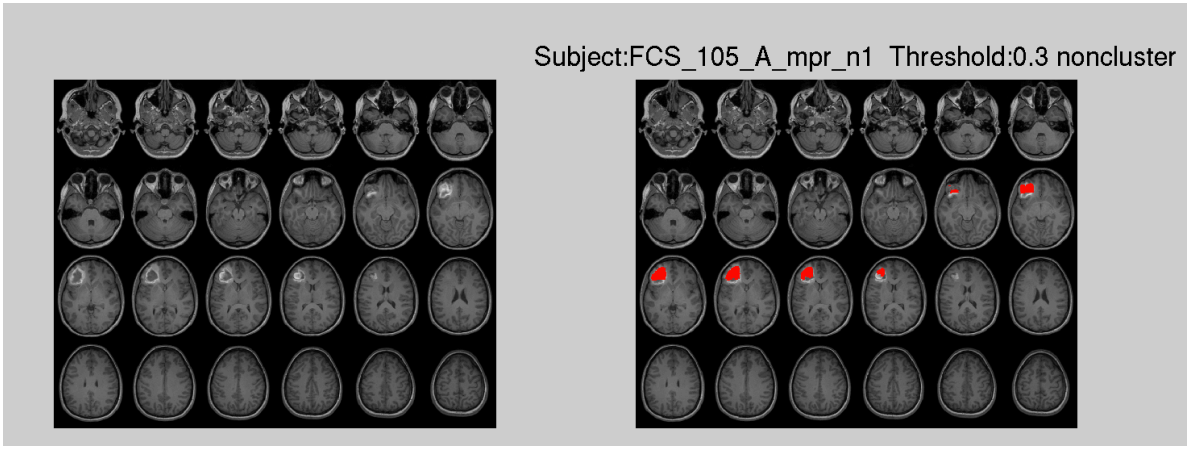

Figure 1.2 Initial lesion result with default threshold (T = 0.3) without clustering for subject 105

We chose to implement a smart clustering method with varying thresholds (ranging from 0 to 1) to improve the identification of the final lesion. Cluster is a gathering of voxels and is defined by similar intensities. If a low threshold is used, multiple clusters are found including many false positives (Figure 1.3 (a)); with a strict threshold only parts of the lesion are identified (Figure 1.3 (b)).

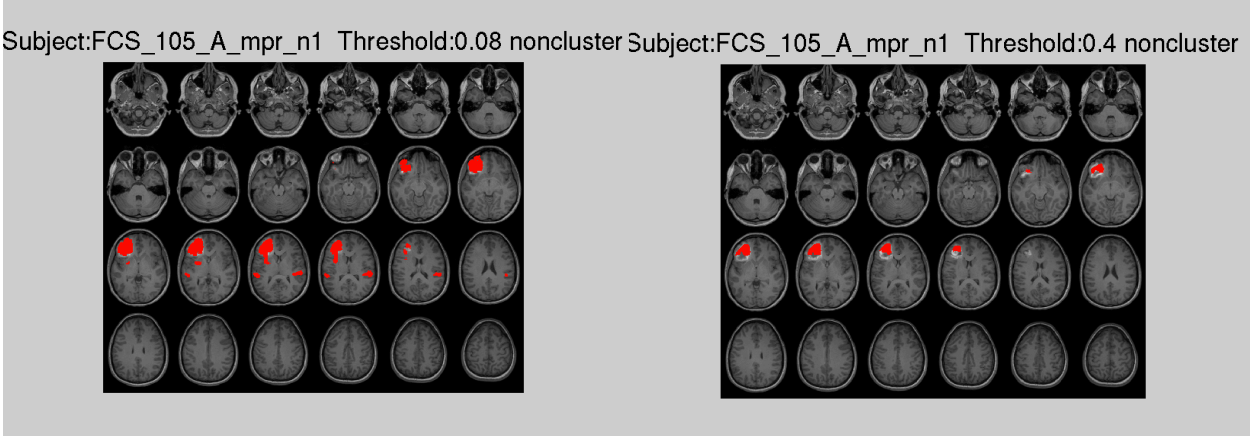

Figure 1.3 Lesion results with: (a) T = 0.08 without clustering; (b) T = 0.4 without clustering

By analyzing the lesion results at low and high thresholds, we realized that the difference between the center of the real lesion and normal tissue is larger than that between false positives and normal tissues. Therefore, we developed a smart clustering algorithm to combine the lesion results generated by different thresholds. We first identified a single lesion cluster x that covers the most distinctive part of the real lesion by setting a strict threshold (T = 0.4). This cluster x is however likely not covering the full extent of the lesion. This cluster is subsequently used to find the correct lesion cluster in lesion files generated by multiple less strict thresholds. For each of these files we extract the five largest size clusters (y_1, y_2, y_3, y_4, y_5), which are the ones that most likely cover the real lesion, and calculate intersection between every cluster y_i ($i = 1,2,3,4,5$) with the strict cluster x, in each lesion file. Using this method we can find the particular cluster y_{real} whose intersection with x is not zero and identify this cluster y_{real} as the actual lesion and the others as noise. With this method we can identify the cluster that is most likely the real lesion for different thresholds, with a cluster that is more likely to cover the extent of the lesion.

Finally, since the segmented lesion is in the template space, we need to transform it into its own space for further study. During registration the local regions are non-linearly matched to the template and the relative locations of these regions within brain have been altered. Since the location of a lesion is as important as the size of a lesion, the lesion is transformed back to its own space for accurate spatial information. The method to implement the re-transformation is done by applying the warp file that we obtained when we employ the nonlinear registration to the generated lesion file.

1.2.6 Interface pipeline

To make these steps user friendly, we developed an automatic segmentation interface that combines the function of the above steps and includes a module to view results with a point and click graphical user interface (GUI) (Matlab, The Mathworks Inc., Natick, MA, USA). With the high variability between patients and lesions, setting a single threshold did not give the best results. This interface allows users to view and compare the different identified lesion results, and make the final decision to extract the real lesion. The automatic segmentation interface (Figure 1.4) is divided into three parts: Subject Selection, Control Selection and Show.

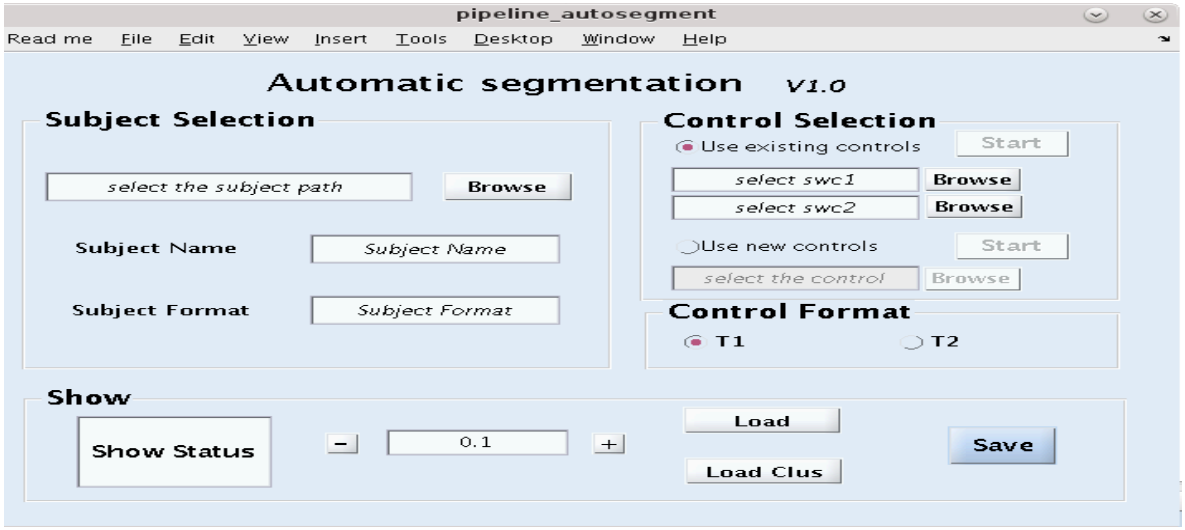

Figure 1.4 Main interface for automatic segmentation

Subject selection: here the structural image of the patient is selected. Either T1-weighted or T2-weighted 4dfp images can be entered.

Control selection: here the control images are selected. For the first use, "Use new controls" should be selected to enter the healthy subjects' brain image. By doing so, all the control subjects will go through the preprocessing, unified segmentation steps as the target patient image. For the second use, since the needed fuzzy set of WM and GM for control group have already been built, user can choose "Use existing controls" at this point, which will save a lot of time by escaping preprocessing and unified segmentation steps. Note: T1-weighted subjects can only be compared with control subjects' T1-weighted images.

Show: after beginning lesion identification by click on "Start" button, the small window in the "Show" panel will present the working status by changing from "Processing" to "Complete ALI". After analyzing the patient data versus the controls the user can use the interface to visually check the results by viewing the lesion overlay on the initial brain image with a separate initial brain image next to it (Figure 1.5). By changing the threshold value through "+" and "-" button and press "Load Clus" or "Load" to choose implementing the smart clustering or not, the user can view the results at different thresholds in the viewing window. After finishing all the comparisons, the "Save" button is used to only obtain the selected lesion file and remove the others (to save space and simplify files).

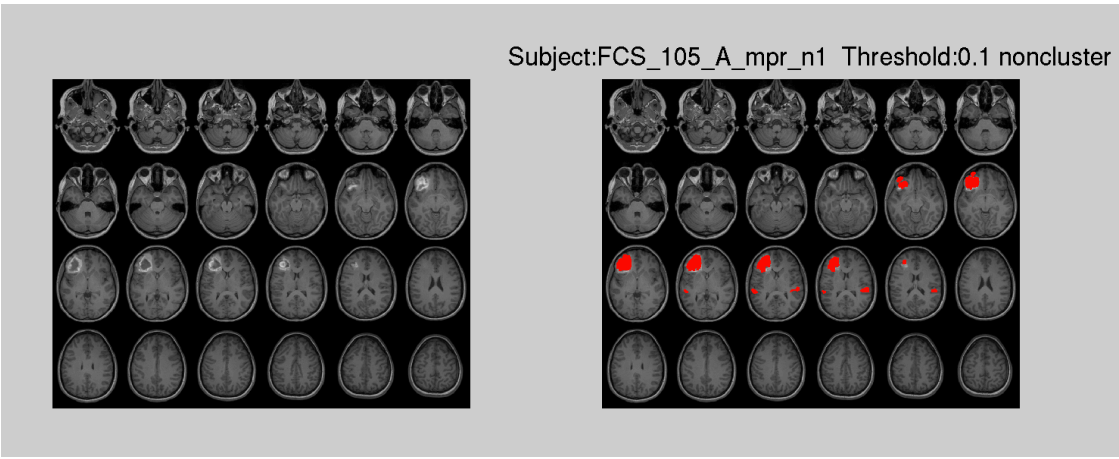

Figure 1.5 (a) Non-clustering result at threshold T = 0.1 for stroke patient 105 for T1 image

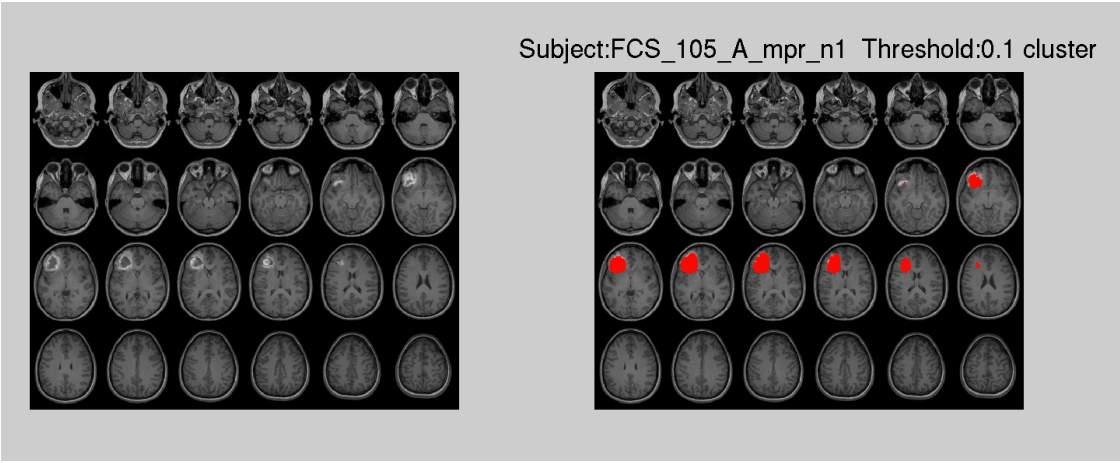

Figure 1.5 (b) Clustering result at threshold T=0.1 for stroke patient 105 for T1 image

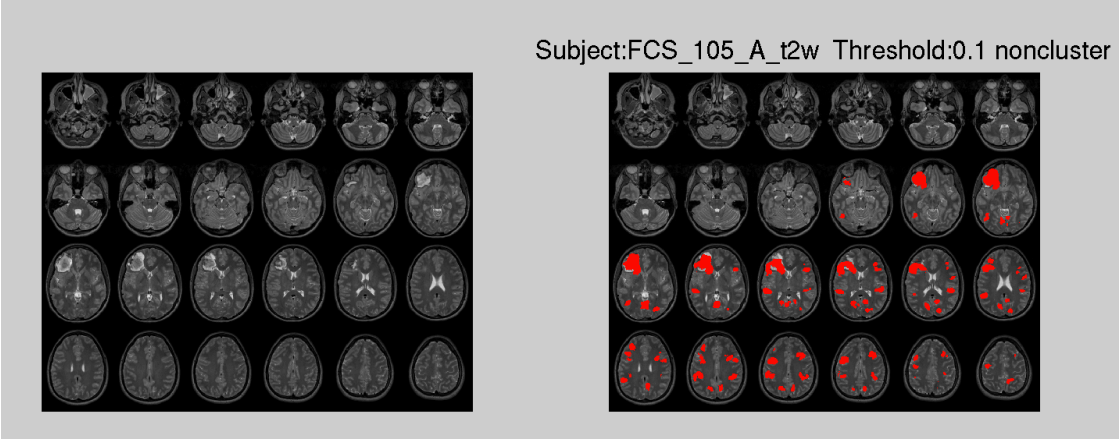

Figure1.6 (a) Non-clustering result at threshold T = 0.1 for stroke patient 105 for T2 image

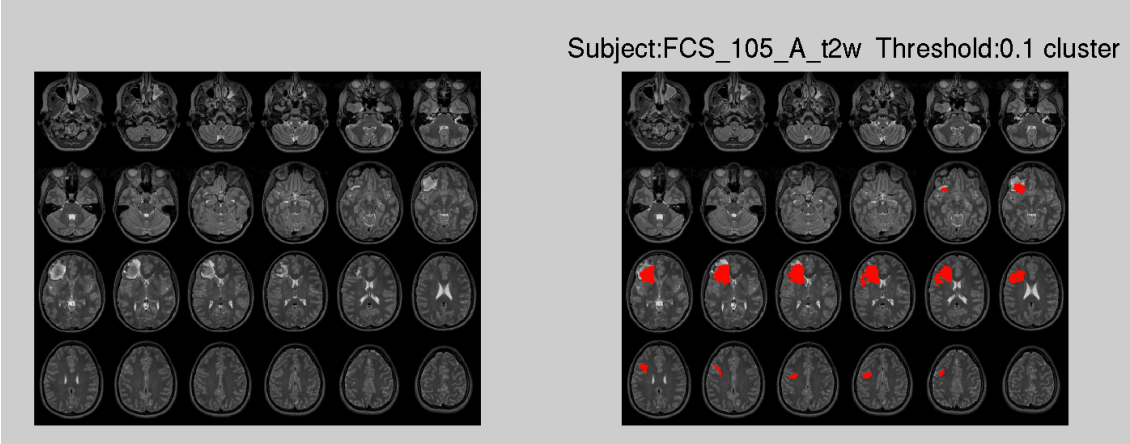

Figure1.6 (b) Clustering result at threshold T = 0.1 for stroke patient 105 for T2 image

1.3 Results

In order to evaluate how the automatic lesion identification method works, the most direct way is to view the lesion result. Figure 1.5 and Figure 1.6 show the identified lesion generated at threshold 0.1 of T1-weighted image and T2-weighted image respectively, both with and without clustering.

The accuracy of the lesion identification method is evaluated by a Receiver Operating Characteristic (ROC) curve (Swets et al. 1979) and similarity index (Dice 1945). In order to test how the automatic segmentation works, we first manually segmented the target brain images for patients. We used the manually segmented lesions as a gold standard to evaluate the difference between the automatic and manually traced lesions.

ROC curves have been widely used in the radiologic community as a tool to visualize the accuracy of detecting Regions Of Interest (ROIs) using different thresholds. In an ROC curve the x-axis represents false positive fraction (FPF)/1-specificity and the y-axis represents the true positive fraction (TPF)/sensitivity. The ROC curve thus takes "hits" and "false alarms" into consideration,

providing an estimation of the overall accuracy. Thus, by looking at the shape of ROC curve we can evaluate the accuracy of this lesion identification method. If the ROC curve is closer to the top left,

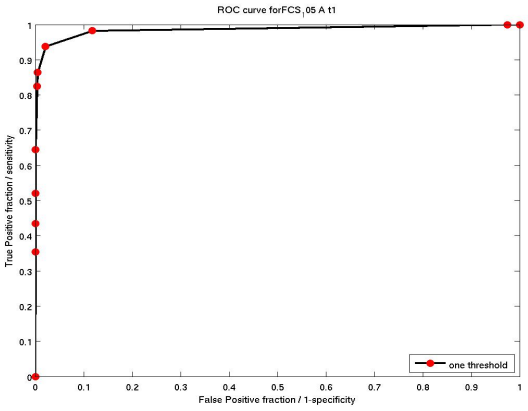

Figure1.7 (a)

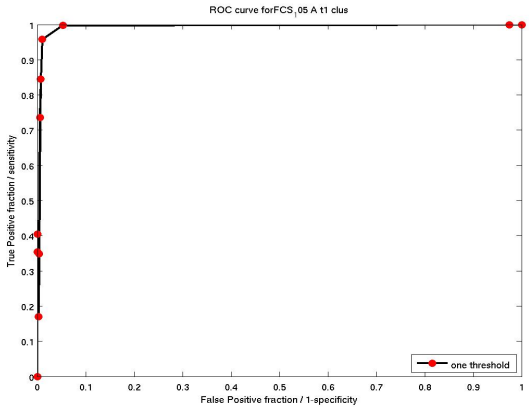

Figure1.7 (b)

Figure 1.7 ROC curve for stroke subject 105: (a) without clustering (b) with clustering

the identified lesion is closer to the real lesion. Furthermore, calculating the area under curve (AUC) is another way to evaluate the ROC curve. The larger the AUC, the better the result. Two examples of the ROC curves for stroke patient 105 (Figure 1.7), without and with smart clustering.

From the ROC and AUC we can get an idea of the accuracy in this particular subject. However, it does not give us a quantitative measurement of which threshold generates the most reasonable lesion result for the subject. A similarity index is introduced to quantify the accuracy of detection. The similarity index is calculated as:

$$\boldsymbol{SI} = \frac{\boldsymbol{2\times(Ref\cap Seg)}}{\boldsymbol{Ref+Seg}} = \frac{\boldsymbol{2\times TP}}{\boldsymbol{2\times TP+FP+FN}} \qquad (1.4)$$

Where Ref represents the reference image (manual) and Seg represents the auto-segmented image. TP, FP and FN are the number of voxels that are true positive, false positive and false negative respectively. The value of similarity index ranges from 0 to 1 and the higher the value, the better the result. Thus we can compare the SI of different lesion results generated by different thresholds in one subject to decide which one works best.

However, SI also has its own limit on evaluating the accuracy. With the high proportion of true positive in the equation, SI focuses more on getting true positives rather than avoiding false positives. For example, although the similarity index of the lesion results for patient 105 in Figure 1.3 generated at threshold 0.1 without clustering and with clustering are 0.63 and 0.40 respectively, we might still want to choose the clustered result (lower SI) because of its low false. Therefore, it is best to use the value of the similarity index in combination with the ROC curve to find the best lesion result.

Figure 1.8 shows an overall result for all subjects without clustering and with clustering. Each dot on the graphs represents the best lesion result for each subject. It is obtained by extracting the lesion result that has highest SI under the condition of FPF less than 0.008 to ensure avoiding false positives. In general, we can see that implementing smart clustering can greatly decrease the FPF and increase TPF.

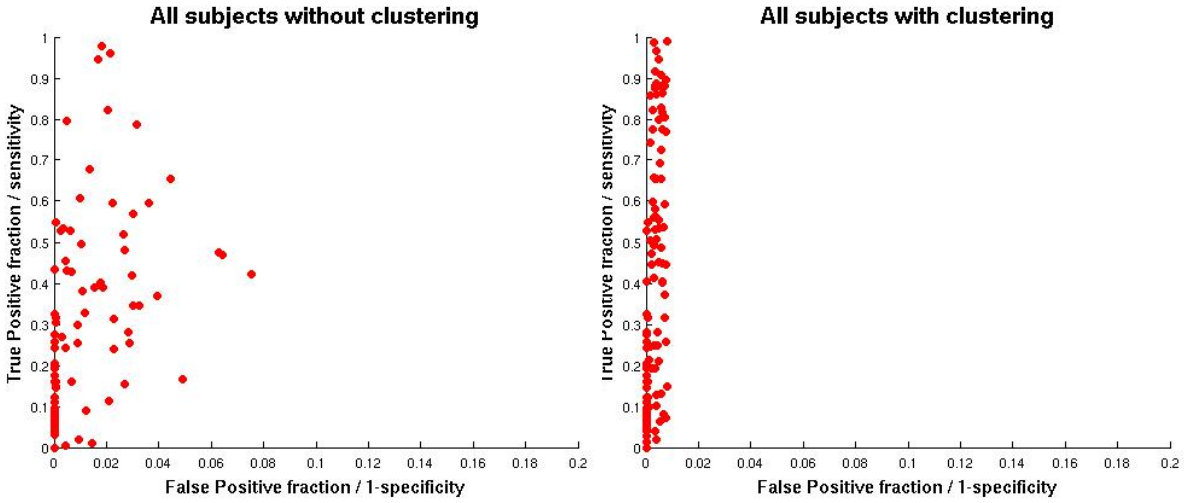

Figure 1.8 (a) **Figure 1.8 (b)**

Figure 1.8 For all subjects obtain the best lesion result: (a) without clustering (b) with clustering

Choosing the best result as mentioned above is however only possible in a set that has been manually segmented. In new patient data this lesion identification method is set to find multiple

solutions that are as close as possible to the ideal solution, but the user has to manually make the final decision using the GUI.

1.4 Discussion

By adding pre-processing and post-processing steps to the ALI toolbox, we developed a pipeline to automatically segment lesion in the brain. This method is compatible for T1 or T2-weighted images. Using the interface, user can conveniently segment and view the results within several clicks. And they can choose which lesion result is most reasonable. The user can then export the lesion result and load it in Analyze biomedical imaging software system ((Robb and Hanson 1991), Wideman-one.com/gw/brain/analyze/formatdoc.htm) to manually refine the result if necessary.

Lesion identification in ALI toolbox is based on finding abnormal tissue in patients as compared to healthy subjects. The high variability of human brains was the first problem we needed to solve in order to avoid identifying normal tissue as lesion, for example due to enlarged ventricles. We added a nonlinear registration that can align the inner regions of brain, e.g. normalizing abnormally enlarged ventricles. This allows for the treatment of the identified differences between healthy subjects and stroke subjects as likely being a part of the lesion.

By analyzing the results that are generated directly after comparison at a default threshold, we found that there was a trade off between identifying only part of the lesion (Figure 1.2) vs. identifying the whole lesion with the inclusion of false positive elsewhere. This trade-off is due to several factors. First, when the size of control group is limited, there is a chance that the range of normal tissue intensities is not well represented in the prior leading to the incorrect classification of that tissue as abnormal. The best way to solve this problem lies in increasing the size of the control group, and restricting other variables that can influence tissue intensity, such as age and gender, to increase the similarity of the control and the patient groups. The second problem occurs when cortical and subcortical structures show high inter-individual variability in size, orientation, topology and

geometric complexity (Thompson et al. 1996) that corresponds to gyral and sulcal geometry variability in the cortex. Obvious inter-subject variations have been reported in primary motor, somatosensory and auditory cortex (Missir et al. 1988; Rademacher et al. 1993), primary and associated visual cortex (Stensaas, Eddington, and Dobelle 1974), frontal and prefrontal areas (Selemon, Rajkowska, and Goldman-Rakic 1995). These problems are likely to inject false positives in the lesion classification. To improve accuracy and limit the influence of these variations we implemented a smart clustering algorithm to obtain the correct lesion cluster that covers as much of the lesion as possible. From Figure 1.7, we can see that clustering moves the ROC curve to the top-left indicating fewer false positive and more true positive after applying smart clustering.

Finally, to provide users more chances to only obtain the complete lesion, we create a user-friendly interface that not only incorporates all the steps, but also visualize flexibly their results for smarter decision. The users can easily view the lesions identified at different thresholds with and without smart clustering. Finally the user identifies the result that is closet to their needs and selects it, which can then be exported and manually edited if necessary. This process gives users more options and increases the accuracy to the best with lowest labor and time cost.

In our study, we assume the precisely manually identified lesion as a gold standard to generate ROC curve and calculate similarity index. After testing more than 100 stroke patients with both ischemic and hemorrhagic etiology, we find that the method works well for lesions located in white matter and grey matter and irrespective of their size. However, since the borders of lesions contain a mix of healthy tissues and damaged tissues, the intensity signal at the border shows less change than at the center (Stamatakis and Tyler 2005). Thus some borders still remain undetected such as in Figure 1.4(b). For small lesions in brainstem and cerebellum (less than 100 voxels), it is difficult to use this method to identify the lesions even with the smart clustering algorithm. Small lesion will have high variability of intensities at the border which decreases the accuracy of this method (Rademacher et al. 1993). Furthermore, as this method identifies the tissue contrast differences between control subjects and stroke subjects, it will regard all detected differences as lesion. For example,

periventricular white matter disease (PWMD) represents a common contrast changes observed in the periventricular white matter of aging subjects putatively due to small vessel damage (Filley 2012). If severe it can cause cognitive decline (Black, Gao, and Bilbao 2009). PWMD is identified as "lesion" using the this method. After applying the smart clustering algorithm, we can eliminate effectively these false positives. Interestingly, in future work this method could be used to identify the severity of white matter disease in subjects with or without lesions.

Future developments could include the use of multi-channel images to implement lesion identification. Finding a way to efficiently combine the separate contrast information from different structural images can be of great potential. T1-weighted and T2-weighted image contrasts result from variation of relaxation time of protons (Hornak 2008), whereas other image modalities focus on different properties of tissues and should also be considered for combined lesion segmentation. For example, diffusion weighted image (DWI) map the magnitude of diffusion of molecules to generate image contrasts from the differences in diffusion rate. Another example is diffusion tensor image (DTI), which can be used to track the trajectory of fibers (WM). These methods could provide us with more information allowing for more accurate lesion identification.

Chapter 2

Spatial shifts in cortical motor representations post-stroke

2.1 Background

2.1.1 Mechanisms of reorganization

In the brain, the motor and somatosensory cortices are somatotopically organized where different regions represent different parts of the body in an organized fashion (the homunculus). Multiple animal and human studies have shown changes in sensory and motor representation after brain injury or amputation of limbs (Cramer and Crafton 2006; Randolph J. Nudo 2006; Kaas and Qi 2004). Interestingly, different changes in neural organization have been observed with different injury models. Two "canonical" injury models have been shown to change cortical representations: (1) peripheral nerve injury, and, 2) damage to the cerebrum itself, either subcortical or cortical (directly to the motor cortex).

The first kind of reorganization focuses on peripheral nerve injury such as limb amputation. This reorganization has been investigated both in humans and animals, and in different target regions: visual (Hubel and Wiesel 1970), somatosensory (Kaas 2000), olfactory (Wilson, Sullivan, and Leon 1987) and motor (Donoghue and Sanes 1987). In general, the lost of afferent input will generate an unresponsive zone in the brain. As time goes on, the regions around the representation of deafferented body parts will move into the "stump region" (that no longer has a function) leading to an expansion of the neural representation for the surrounding preserved body parts. There are also

local alterations of connections between the "stump region" and neighboring (preserved) regions with the formation of new connections through axonal or dendritic sprouting (Navarro, Vivó, and Valero-Cabré 2007; Kaas 2000; Kaas and Qi 2004). The functional consequences of this neural reorganization are not entirely clear. Stimulation of the "stump region" leads to peripheral responses of neighboring body parts which would suggest that the stump is now partially controlling non-deafferented body parts possibly through novel intracortical connections verified by bidirectional tracers and electrophysiological recording (Florence et al. 1998). The functional shift into the "stump region" (refocusing) is not limited to the motor system, visual deprivation also lead to a compensatory increase in the representation of selective somatosensory inputs, for example, somatosensory stimulation in blind people can activate parts of the visual cortex (Cohen et al. 1997). These changes are likely due to increased learning and training in the preserved somatosensory inputs after losing one input, supporting the idea that cortical organization is dynamically remapped during learning and experience (Donoghue, Hess, and Sanes 1996).

The second kind of reorganization focuses on central nervous system injury such as cerebral lesions. Cerebral lesions can directly damage the neurons, e.g. as in a lesion of motor cortex, while subcortical lesions can affect function by disrupting the connections from the motor cortical representation site to the body, e.g. as in a lesion of the cortico-spinal tract fibers. In both cases patients can present with an enlargement or shift of the limb representation in the cortical area to the surroundings (Randolph J. Nudo 2006; R. Chen, Cohen, and Hallett 2002).

After a cortical stroke the reorganization happens with neuroanatomical alterations in both adjacent and remote cortical tissues. Locally the functions of the lesioned area shift to peri-infarct regions (Randolph J. Nudo 2006), which means the surrounding regions will partially take over the function of the damaged one. Immediately after the stroke this shift occurs through unmasking of existing but inactive pathways and through the formation of new synapses (Fisher 1992; Ago et al. 2003). Over time axonal regeneration and sprouting, which are supported by sequential waves of expression of growth-promoting genes after a focal infarct in the motor cortex (Carmichael et al.

2005), play a role in consolidating this functional shift (R. Chen, Cohen, and Hallett 2002). Therefore both recruitment of existing pathways and generation of new connections between the damaged area and its surroundings make the shift of damaged representation possible.

Unlike after a cortical stroke, the damage caused by subcortical lesion can be more diffuse due to damage to white matter tracts, which might affect a larger cortical area. Although the actual mechanism of reorganization after subcortical stroke is still unclear, we think that in patients with some residual motor function, the changes caused by a subcortical lesion are similar to both mechanisms presented. Similar to complete deafferentiation the cortical regions representing the limb tested completely lose their effect. However, like in cortical lesions, there is no complete deafferentiation there are chances patients can re-gain control of the corresponding body parts by unmasking existing pathways and forming new connections with surrounding brain regions. Several studies have investigated the remapping after subcortical stroke but the results have been varied.

Neuroimaging (fMRI, PET) studies found that hand movements of the affected limb cause a posterior shift of the geometric center of cluster activation in ipsilesional sensorimotor cortex in patients with subcortical ischemic stroke (Pineiro et al. 2001; Calautti et al. 2003). Posterior displacement of sensorimotor responses was also demonstrated in a group of patients with multiple sclerosis and damage of the corticospinal tract (Lee et al. 2000), as well as in patients with spinal cord injury (Green et al. 1998). Thus a posterior displacement in motor (sensory) peak response could be an index of relative deafferentation of the motor cortex.

In contrast, a magnetoencephalography (MEG) study reported an ipsilesional activation shift along the medio-lateral axis of the hand region in a group of three subjects, and recruitment of regions outside of hand area in three other individuals (Altamura et al. 2007). In relation to recovery, a transcranial magnetic stimulation (TMS) experiment found that after subcortical stroke better motor outcome correlated with a larger stimulation area in the whole group of stroke subjects (N = 27),

and a correlation between motor outcome and map shift in a subgroup of subjects (N = 10) with normal corticospinal conduction (Thickbroom et al. 2004).

In summary, the brief review highlights that the human correlates of spatial shifts in motor representation demonstrated so clearly in animals studies are far from clear. Shift along medio-lateral axis may represent a shift within motor cortex possibly reflecting the recruitment of neighboring body part representations, while an anteroposterior shift might indicate the recruitment of nearby non-primary motor areas with direct corticospinal projections, such as premotor cortex or pre-central cortex or increased excitability of connections between these areas and primary motor cortex (Byrnes et al. 2001). The reasons behind this variability are many including variability of methods, small sample sizes with variable lesion location and size, motor impairment, etc.

In the second analysis of my thesis I will focus on the question of possibly remapping of cortical motor representations post-stroke. This study has several advantages over previous studies. First, the sample size (N = 132) is larger than that in other studies. Secondly, we use a method based on resting state fMRI that maps all the connections between one area and the rest of the brain, not just highlights the peak of motor activation. Thirdly, our strategy involves a signal, i.e. the inter-hemisphere correlation of the fMRI signal time series between the normal and the damaged precentral-postcentral region of the brain, which allows for a topographic mapping of possible shifts in representation, as well as recruitment of additional premotor or sensory regions.

2.1.2 Hypothesis

We plan to measure the inter-hemispheric temporal correlation, as known as functional connectivity (FC) of the fMRI signal measured at rest between the normal hand motor representation (knob region) and damaged pre-central/post-central region in a group of stroke patients with motor deficits. We hypothesize the inter-hemispheric FC will show acutely a spatial shift along anterior-posterior axis to other non-motor region, or a medial-lateral axis to nearby face or leg region because of the unmasking of existing but inactive pathways. This will allow to separate a mechanism based

on shift within the motor cortex versus recruitment of accessory premotor/sensory regions. As the newly unmasked the lateral connections are more diffuse, the intensity of the highest connectivity on the damaged hemisphere might decrease. Furthermore, we hypothesize that the extent of the spatial change will have a relationship with the severity of the damaged function.

During the recovery process, especially for patients who have recovered well from motor deficits, we hypothesize the formation of new connections that compensate for the damaged ones, and that may appear as a spatial shift of FC consistent with a chronic recruitment of cortical regions outside of motor cortex. Moreover, we hypothesize a positive correlation between motor outcome and the degree of cortical shift.

2.2 Methods

Functional MRI (fMRI) measures blood oxygenation level-dependent (BOLD) signal, which is an indirect measure influenced by variations in blood flow, blood volume, and oxygenation that are related to neuronal activity and metabolism (Kim and Ogawa 2012). To avoid confounds related to behavioral deficits, i.e. patients with different level of deficits may generate different levels of motor activation when moving their weak limb, we choose to use resting-state fMRI (rsfMRI), a method based on the temporal correlations of spontaneous BOLD signal fluctuations while subjects rest quietly in a scanner (Greicius et al. 2009). During resting state, it has been shown that homologous connections of left and right primary motor network are somatotopic organized and that corresponding regions are highly correlated (Van Den Heuvel and Pol 2010). During our data collection behavioral measures of motor, sensory, language and cognitive abilities were gathered. For the current work we chose a dedicated arm score to measure motor deficits. In addition, since previous studies (Grefkes and Fink 2011; Volz et al. 2014; Jang et al. 2014) as well as our own data show a clear correlation ($p<0.05$) between motor deficit and cortico-spinal tract (CST) damage, we also combine the extent of CST damage with the measures the motor function. The analyses were carried out using Connectome DataBase and Connectome Workbench (Human Connectome

Project, Washington University in St. Louis, http://www.humanconnectome.org/). The statistics were done using IBM SPSS statistics (Statistical Package for the Social Science, IBM corportation, Armonk, New York, US) and Matlab (The Mathworks Inc., Natick, MA, USA).

2.2.1 Data acquisition

We use rsfMRI scans from same database as indicated in 1.2.1, of 132 stroke patients and 27 healthy age-matched controls (AMC). Data was collected in the stroke patients at 3 time points (2 weeks, 3 months, 1 year after stroke respectively) and data of AMC subjects was obtained at 2 time points, 3 months apart. The functional MRI data underwent preprocessing steps demonstrated in Baldassarre (Antonello Baldassarre et al. 2014) and are as follows: 1) compensation for asynchronous slice acquisition using sinc interpolation; 2) elimination of odd/even slice intensity differences resulting from interleaved acquisition; 3) whole brain intensity normalization to achieve a mode value of 1000; 4) spatial realignment within and across functional MRI runs; 5) resampling to 3 mm3 voxels in atlas space including realignment and altas transformation in one resampling step. The behavioral scores were obtained from the database in 1.2.1 as well. The arm deficit score is measured using the ARAT (Action Research Arm Test) with a range of 0 to 1 (after normalization) while the composite score was derived from a number of measures of range of motion, strength as well as dexterity for both upper and lower extremity. A principle component analysis was used to reduce number of variables (Corbetta et al. 2015). The number of voxels damaged in CST was measured by multiplying the probabilistic map of cortico-spinal tract (CST) with the lesions. The tract probability map is generated using diffusion tensor image (DTI) from 40 healthy subjects (A Baldassarre et al. 2016).

2.2.2 Surface based registration

The majority of fMRI studies measure BOLD signals in a volume space, which means each voxel is registered to its actual anatomical 3-D position. We chose a more accurate method based on computerized cortical surface representations (Drury et al. 1996; Bruce Fischl et al. 1999; Van Essen et al. 2001; Wandell, Chial, and Backus 2000; Schwartz, Shaw, and Wolfson 1989), which allows for

surface registration and surface manipulations. This method is advantageous over volumetric approaches because each vertex on the surface is much more consistently aligned across individuals and has been transformed to a 2D surface that is not affected by re-sampling and spatial normalization. It is realized by inflating the brain into a sphere to retain the location of the sulci and gyri. Then registering the vertices of the single subject brain sphere to a template atlas sphere, which is then transformed back to a brain (Glasser et al. 2013). The surface based method contains more complete data and is more effective in reducing inter-subject variability (B Fischl, Sereno, and Dale 1999). Considering our large and varied subjects pool using a consistent criterion across individuals is especially important.

2.2.3 Seed-based approach

After obtaining the fluctuations of BOLD signal in certain time period of the whole brain, we defined a seed in the brain as the target region. In this study the rsfMRI approach is based on the observation that homotopic cortical regions are strongly connected in healthy subjects. The goal was therefore to compare the strength and spatial topography of homotopic motor connections from a seed region in the "hand knob" (Yousry et al. 1997) of the normal hemisphere to the contralateral pre-central/post-central regions. The hand knob in each hemisphere was identified on the atlas and can be seen in yellow in Figure 2.1. The identified vertices were then used to select this hand region in our patients and controls. Through visual inspection this seed area matched well in individual healthy subjects and stroke patients. Four example subjects are shown in Figure 2.2.

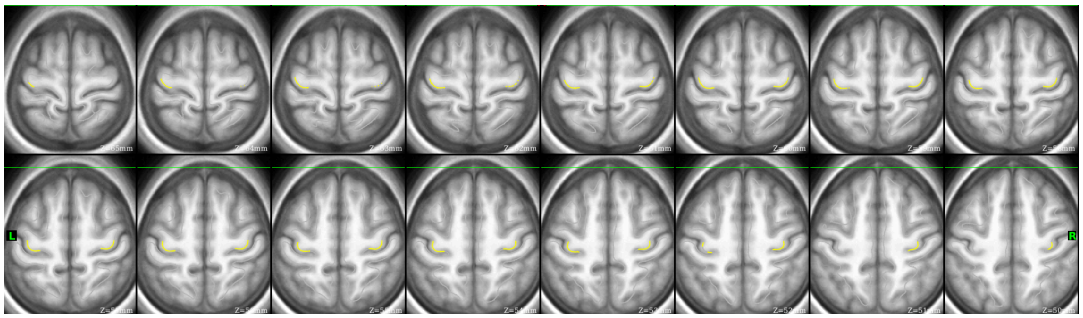

Figure 2.1 Seeds covering hand knob on both sides

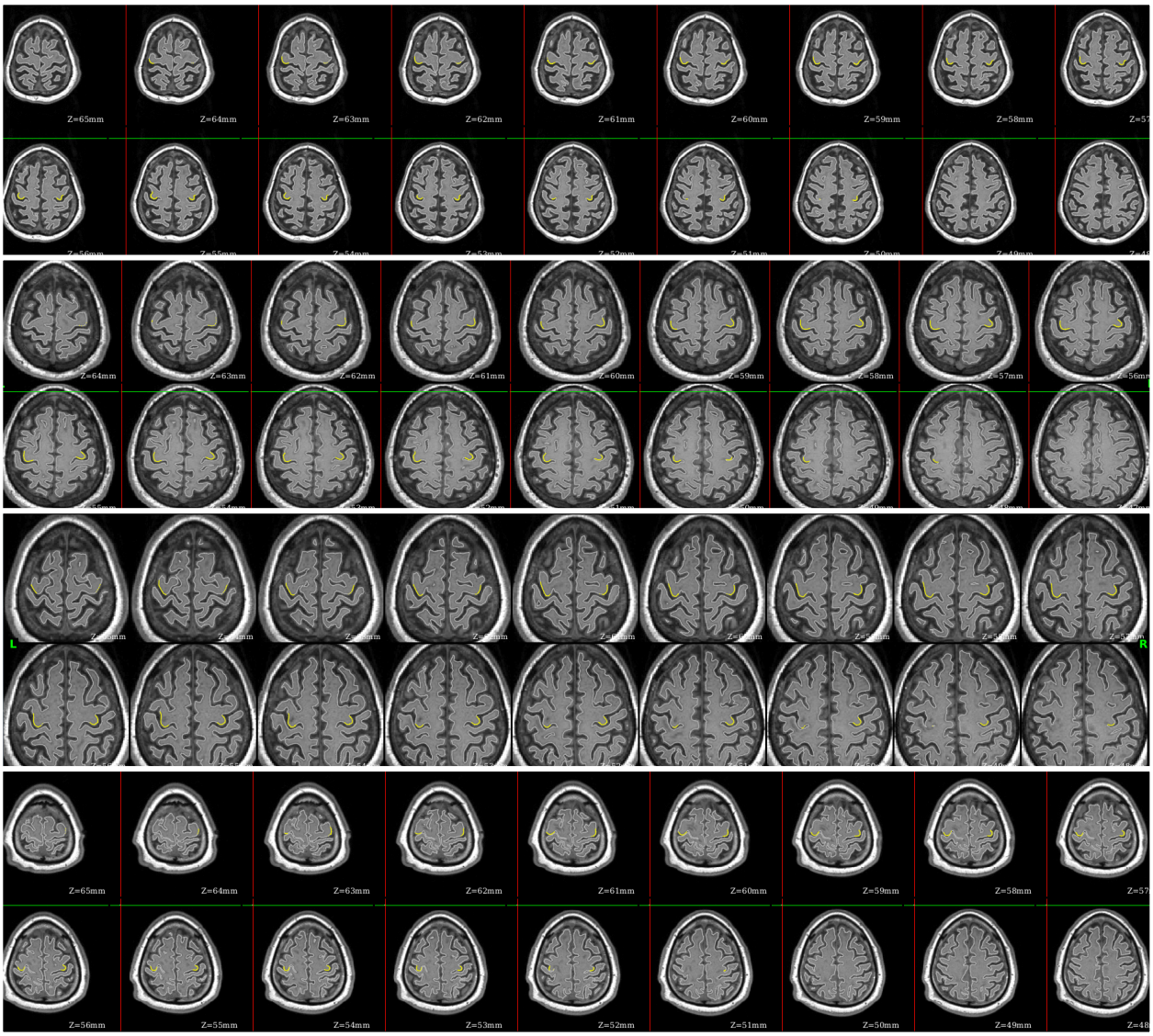

Figure 2.2 Atlas generated hand knob seeds overlay on 4 subjects (from top to bottom: healthy subject 004, 010, stroke patient 067, 168)

Seed correlation map was computed by extracting the time course for the seed and computing the correlation coefficient (Pearson r) between that time course and the time course from all other brain vertices. Then the Pearson correlations went through Fisher z-transform to generate z(r) seed map (Antonello Baldassarre et al. 2014). Here, the seed placed is placed in the undamaged hemisphere to

generate correlation maps of both the undamaged and damaged hemisphere. Then it can be used to evaluate the location and intensity of highest correlation in the lesion-affected hemisphere, which we assume to be the new hand representation.

Figure 2.3 is the correlation map of control subject 003 for the left and right hemispheres when the seed, which marked in green, is placed on the left hemisphere. The colors of the brain surface represent the correlation value with respect to the seed. Regions in yellow have stronger temporal correlation with the hand knob region.

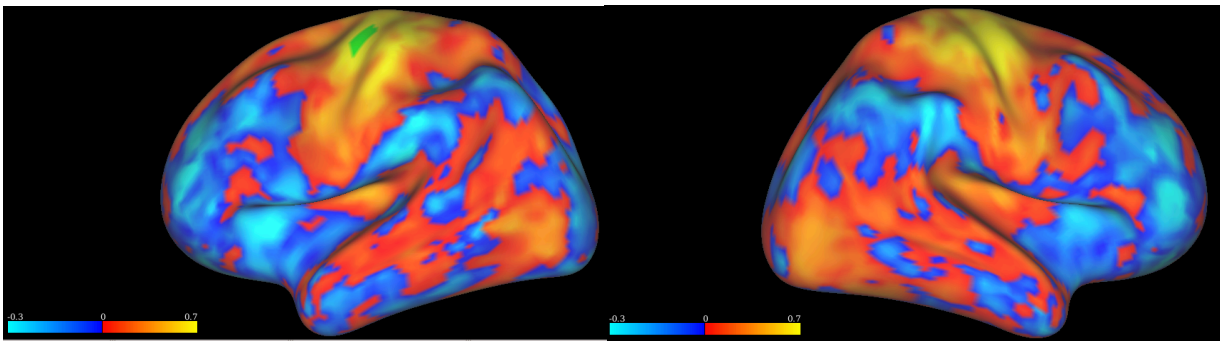

Figure 2.3 Left and right hemisphere correlation maps for control subject 003

To reduce noise (and the number of comparisons) we limit our search region to the area around the central sulcus. The parcelation of Gordon et al (Figure 2.4) was used to select the parcels of the pre and post central gyrus (Gordon et al. 2014).

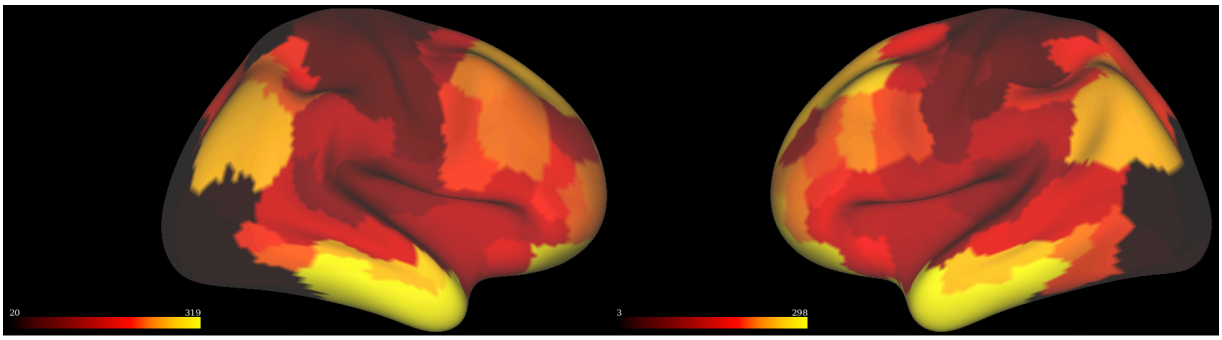

Figure 2.4 Cortical area parcellation based on resting state correlations

We extracted the regions that cover the pre and post central gyrus and make a central sulcus mask that contains 982 vertices, as shown in Figure 2.5(a). Figure 2.5(b) shows the central sulcus correlation map for control subject 003 after applying this mask on the right hemisphere.

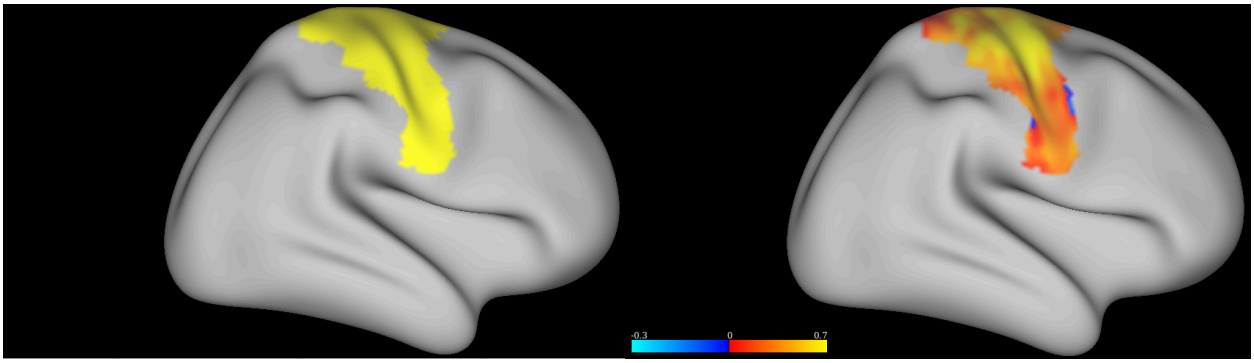

Figure 2.5 (a) Central sulcus mask **Figure 2.5 (b) Central sulcus correlation map for control subject 003**

2.2.4 Peak analysis

After obtaining the region map within the central sulcus on the damaged hemisphere, the first method to analyze the spatial shift of the sensorimotor region is to implement a peak analysis. This method identifies vertex within the mask that has the highest correlation with our seed in the undamaged hemisphere. To decrease fining local maxima that are caused by noise we clustered the correlation maps and identified the vertex with the highest correlation within the largest cluster. To cluster the data, we first normalized the vertices in central sulcus region to generate a z-scored correlation map (mean = 0; standard deviation = 1). Then we sorted the vertices of this z-scored map according to their correlation intensities in ascending order. We extracted the correlation value of the 99% percentile in this map and delete the vertices whose correlation intensity is below this correlation value. The remaining vertices are the ones with the highest 5% correlation value in the central sulcus. Next, we clustered those vertices using Human Connectome Workbench (Marcus et al. 2011) to separate the vertices into different groups based on their spatial location. After that, we picked the largest size cluster and define the peak vertex within this cluster as real peak vertex with respect to the hand knob on the undamaged hemisphere. At this point, we can use the index of this

vertex to get corresponding X, Y and Z coordinates (Talairach and Tournoux 1988) and evaluate the spatial change.

2.2.5 Region analysis

As a second analysis we investigated the intensity change around hand area in the damaged hemisphere, done through a region analysis in different groups (within stroke patients: motor deficit group and no deficit group). Instead of only analyzing the correlation value for one vertex, we generated a circle region around the real peak vertex with a radius of 2cm. Depending on the exact location this includes approximately 100 vertices. For each subject, the values within the sphere are binned to get the frequency of each value. Next, for all the subjects in a group (deficit or no deficit), the vertices within the circles are combined based on the ratio's of the frequencies to correct for the different number of vertices for each subject and the size of groups. Thus instead of directly summing the times of occurrence for different intensity values, we calculate frequencies in each subject and combine them to get a distribution of the intensities in the circle for all the subjects in that group (finally divided by the number of subjects in the group) avoiding the influence of different vertex numbers in the circle for different subjects.

2.3 Results

The analysis of the spatial shift of peak vertex and the intensity change of the region surround peak vertex are done separately at the acute stage and during recovery, in order to investigate the changes shortly after stroke as well as the changes during recovery.

2.3.1 Acute stage

Acutely, changes in the brain were investigated two weeks after stroke. The images of patients with lesions in the left hemisphere are flipped (Left to Right) to align all lesions onto the right hemisphere. We then placed the seed in the undamaged left hemisphere and identified the peak

vertex in the right hemisphere for all subjects (both control and stroke) using the described peak analysis. Then for each subject we plotted its x (left, right), y (anterior, posterior), z (ventral, dorsal) coordinates of the peak vertices, which can be seen in (Figure 2.6).

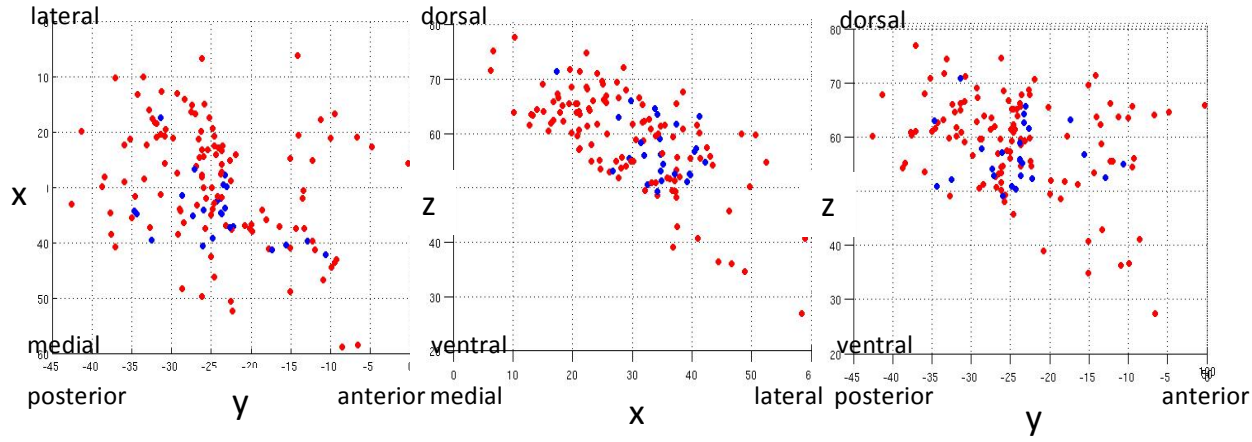

Figure 2.6 (a) X-Y axis **(b) X-Z axis** **(c) Y-Z axis**

Figure 2.6 Coordinates of peak vertices for healthy subjects (blue) and stroke patients (red)

Blue dots represent healthy subjects (AMC controls; N = 27) and red dots represent stroke patients (N = 127). From Figure 2.6 above we can see that the blue dots are in the center of the red dots population in each of the three directions. It directly shows the increased variance of the location of stroke patients' peak coordinates compared to healthy subjects. When we ran independent samples t-test on these two groups along three directions, a significant difference is shown along the X axis (df = 152, p = 0.008) while along Y axis (df = 152, p = 0.900) and Z axis (df = 152, p = 0.132) difference were not significant. Therefore, acutely after stroke there is a spatial shift of the peak coordinate of inter-hemispheric FC, especially along the primary motor cortex (X axis: medial-lateral) in the damaged hemisphere for stroke patients compared to healthy subjects. The distribution (Figure 2.6(b)) suggests that the peak of the FC is located more medially and dorsally, as in a shift toward the leg representation from the original hand knob.

The large difference of group size between the AMC and stroke group could bias the results and there is a higher chance that stroke patients' brain images contain more noise than those of healthy subjects. Therefore, instead of using the AMC subjects as control group, we chose to form a new control group consisting of stroke patients who do not have motor deficits and no CST damage. Based on the ARAT behavioral score and the degree of CST damage, we categorized our stroke patients into two groups: motor deficit with CST damage (motor deficit group; N = 51), and no motor deficit with no CST damage (no motor deficit group; N = 41). Patients with lesions in the "hand knob" region, no motor score or CST damage were excluded. Table 2.1 shows the two groups' peak vertices' coordinates.

Table 2.1 Peak vertices' coordinates comparison for motor deficit and no deficit

Peak vertices' coordinates	Group	N	Mean/mm	Standard Deviation (Std.)	Std. Error mean
X	Motor deficit	51	26.22	13.42	1.88
	No motor deficit	41	30.81	8.27	1.29
Y	Motor deficit	51	-23.02	8.78	1.23
	No motor deficit	41	-24.15	7.36	1.15
Z	Motor deficit	51	60.07	10.72	1.50
	No motor deficit	41	58.51	6.53	1.10

The peak vertices of the motor deficit group are more variable than the no deficit group, especially in the X and Z directions, which can be seen as the large difference of standard deviation. The independent sample t-test between these two groups showed a trending significant difference along X axis ($df = 90$, $p = 0.058$) while the other two directions did not (Y: $df = 90$, $p = 0.512$; Z: $df = 90$, $p = 0.415$). Therefore this analysis confirms that the acute FC peak in the damaged motor cortex is

shifted in the X direction (more medially) both as compared to healthy subjects and a group of stroke subjects without motor deficits. While analysis of peak locations using directional values seek for a consistent shift in a give direction, the variability of lesions that can cause more motor deficits and the observation of consistently higher variance in the stroke group led us to consider the possibility that motor deficits are associated with more variability in cortical motor representation. Therefore, next we measured whether high variance in the motor deficit group was a result of spatial shift away from the normal peak (independent of direction). We calculated an ideal peak vertex coordinate (34.29, -24.22, 56.50) in the damaged hemisphere by averaging all the healthy subjects' peak vertex coordinates. Then we calculated the absolute distance away from the ideal peak for all the subjects. Figure 2.7 shows the motor deficit group in red and no deficit group in green.

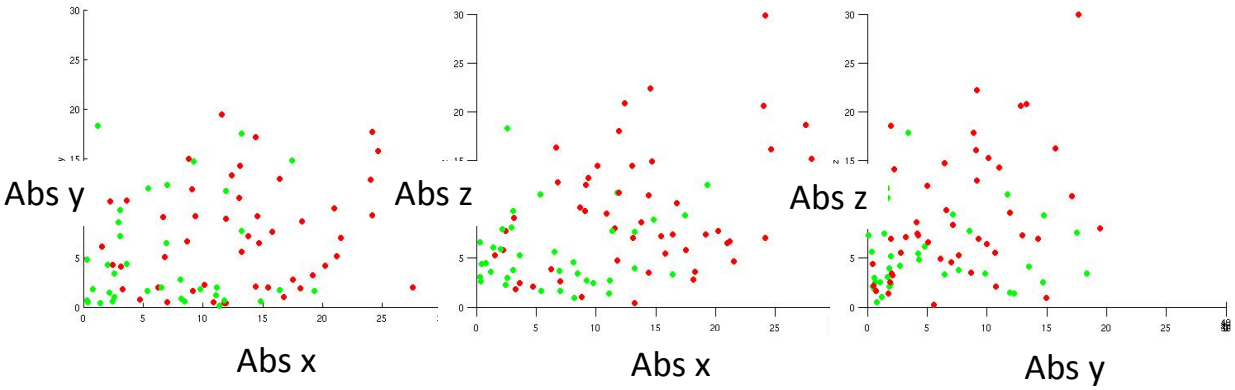

Figure 2.7 (a) X-Y axis **(b) X-Z axis** **(c) Y-Z axis**

Figure 2.7 Absolute distances of peaks away from ideal peak for motor deficit and no deficit subjects (green: no motor deficit, red: motor deficit)

The green dots (no motor deficit) are closer to the zero point than the red dots (motor deficit), indicating that a spatial shift away from the idea peak in the motor deficit group. Independent samples t-test on the absolute distance from ideal peak confirmed this impression: X axis ($df = 90$, $p < 0.001$), Y axis ($df = 90$, $p = 0.050$) and Z axis ($df = 90$, $p = 0.001$). To further test the difference of absolute distance away from ideal point for two groups, we performed a Permutation test on three axes respectively. First, the standard deviation of the two groups was calculated separately as

std1 and std2 and the ratio of std1 over std2 was calculated and labeled as the "real ratio". For the permutations subjects in the two groups were randomly assigned to a permuted deficit (1) vs. no deficit group (2). This procedure was repeated 10000 times. Finally we calculated the mean and standard deviation of the 10000 ratios and compared "real ratio" with the permutation mean ("mean") and standard deviation ("std"):

$$|\boldsymbol{real\ ratio - mean}| = \boldsymbol{n \times std} \quad (2.1)$$

If n is greater than 2, the difference of the peak variance between the two groups in this axis is significant. The x, y, z axis result are shown as Figure 2.8(a)(b)(c).

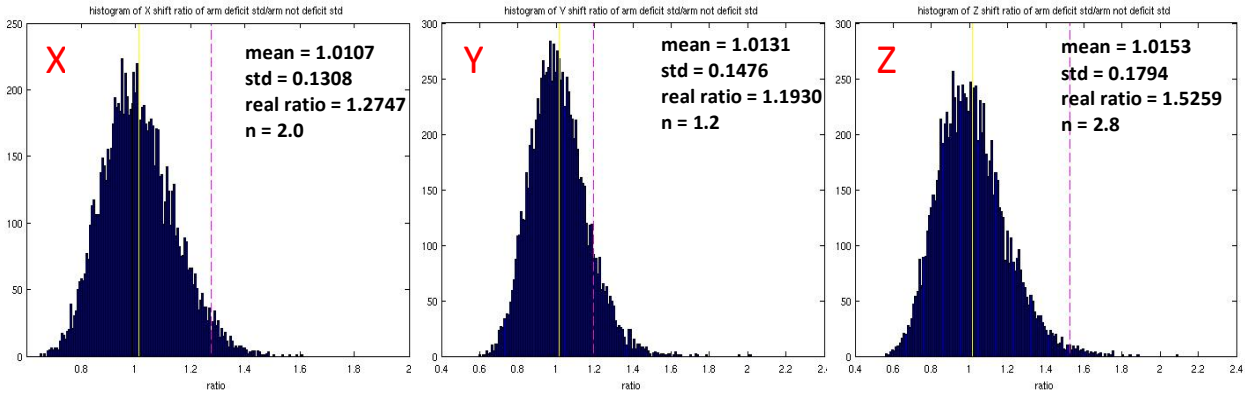

Figure 2.8 (a) X axis **(b) Y axis** **(c) Z axis**

Figure 2.8 Permutation of variance along three axes for motor deficit and no deficit groups

The red line is the "real ratio" and yellow line signifies the permutation mean. We can see that for axis X and Z, n is greater than 2, which indicate that the peak variance between the two groups along X and Z axes are significantly different. This shows that the peak vertices of motor deficit stroke patients are more variable in the X and Z direction compared with no deficit stroke patients. The results validate our hypothesis that stroke patients with motor deficits show spatial change of peak location within the motor cortex, along the medial-lateral (x) and ventral-dorsal (z) axes.

The behavioral validity of these FC correlates was examined by correlating the degree of acute spatial shift with motor behavioral scores in the whole stroke patient group (N = 127), we found a

significant correlation (r = 0.2, p = 0.014) between X directional shift and ARAT score, while not in Y (r = -0.090, p = 0.274) and Z (r = -0.074, p = 0.367) direction. For patients with motor deficits (N = 51), we did not find any significant correlation with the directional shifts along X axis (r = -0.004, p = 0.972), Y axis (r = -0.112, p = 345) and Z axis (r = 0.059, p = 0.621). However, when we examined the correlation with absolute values and Euclidean distances from the ideal peak, we found a significant correlation. Figure 2.9 maps the correlation between the ARAT score and the absolute distance away from ideal peak along (a) x axis (r = -0.206, p = 0.080); (b) y axis (r= -0.302, p = 0.009); (c) z axis (r = -0.216, p = 0.066) and (d) Euclidean distance (r = -0.331, p = 0.004). Patients with more severe motor deficits have FC peaks that are farther away from the ideal peak in the damaged hemisphere.

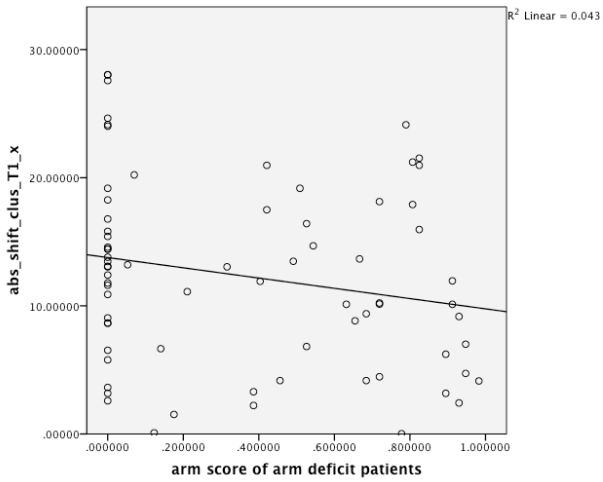

Figure 2.9 (a)

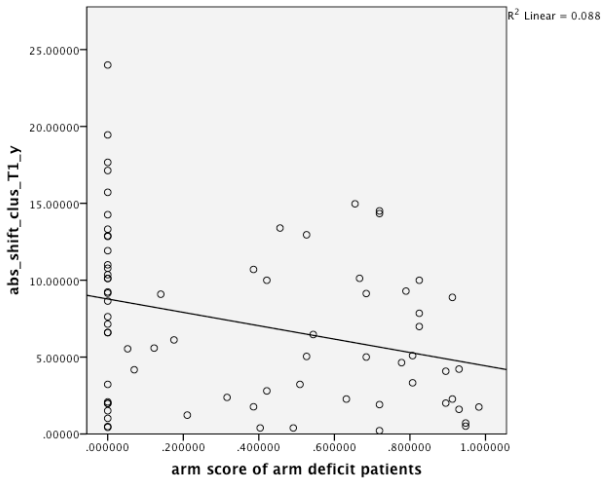

Figure 2.9 (b)

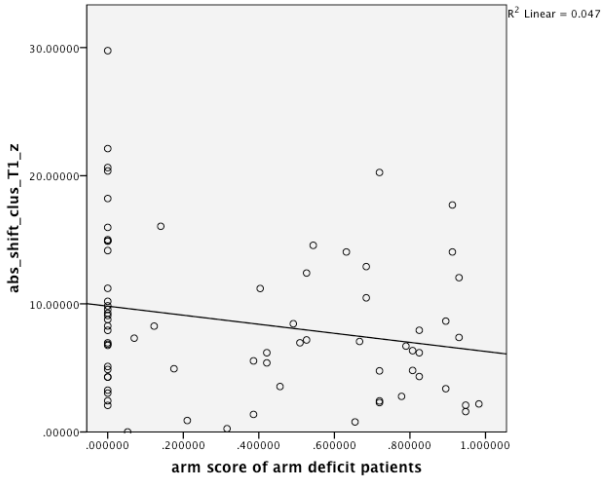

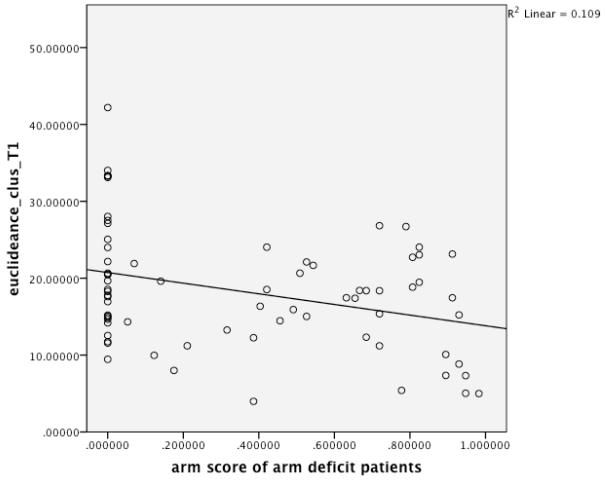

Figure 2.9 (c) **Figure 2.9 (d)**

Figure 2.9 (a) Scatter plot of arm score versus absolute x distance away from ideal peak
(b) Scatter plot of arm score versus absolute y distance away from ideal peak
(c) Scatter plot of arm score versus absolute z distance away from ideal peak
(d) Scatter plot of arm score versus Euclidean distance away from ideal peak

In summary, this analysis shows a relationship between severity of motor deficits and variability of the topography of FC homotopic motor connectivity. The significant correlation with absolute values and Euclidean distance, but not directional values, suggest that the correlation between peak shift and behavior outcome might not be restricted in a particular direction, but the size of the shift is more important for the behavioral deficit.

In addition to the analysis of the peak homotopic FC, we examined the relationship with the strength of inter-hemispheric FC using the region based analysis described in the methods. The intensity of FC was evaluated in a spherical region that includes the peak and that contains approximately 100 vertices. Figure 2.10 shows that the mean value of intensity for the motor deficit group is lower than that for the no deficit group, while the standard deviation of intensity is higher in motor deficit group. This directly shows a decrease of functional connection strength of the hand region on the damaged hemisphere for the motor deficit group, which is accordance with our

hypothesis. The high variance might be caused by the different degrees of motor damage within motor deficit group.

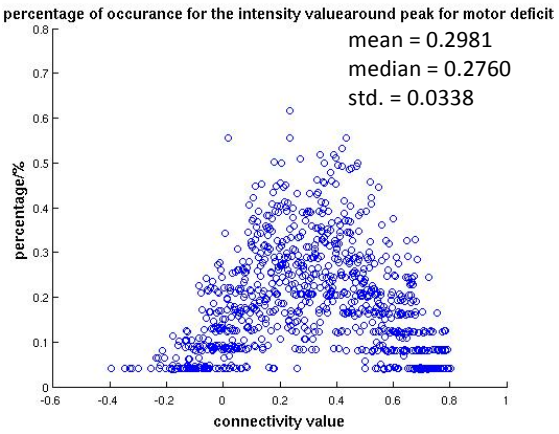

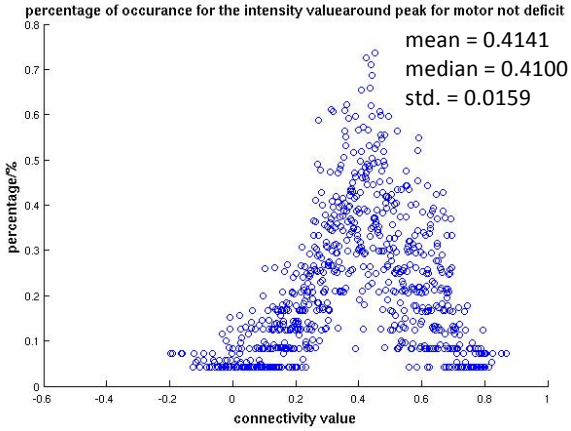

Figure 2.10 (a) **Figure 2.10 (b)**

Figure 2.10 (a) Percentage of occurrence for intensity value around peak for motor deficit group
(b) Percentage of occurrence for intensity value around peak for the no deficit group

We also investigated the relationship between the peak location and the peak intensity. There was no significant correlation along X axis ($r = 0.137$, $p = 0.091$), Y axis ($r = 0.126$, $p = 0.120$) and Z axis ($r = -0.137$, $p = 0.090$) between the directional shift size and peak intensity. However, when we looked at the relationship between absolute shift and peak intensity there was a significant correlation along all axes: X axis ($r = -0.417$, $p < 0.001$), Y axis ($r = -0.347$, $p = 0.000$), Z axis ($r = -0.362$, $p < 0.001$) and Euclidean distance ($r = -0.507$, $p < 0.001$).

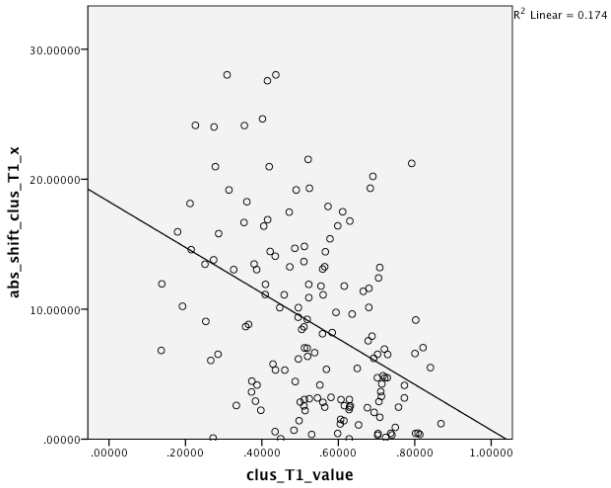

Figure 2.11 (a)

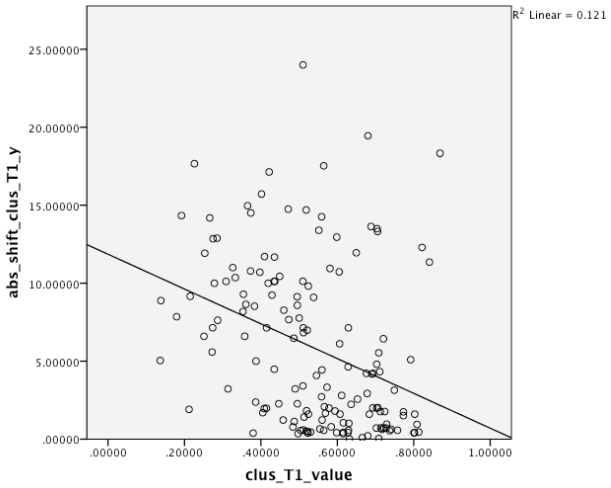

Figure 2.11 (b)

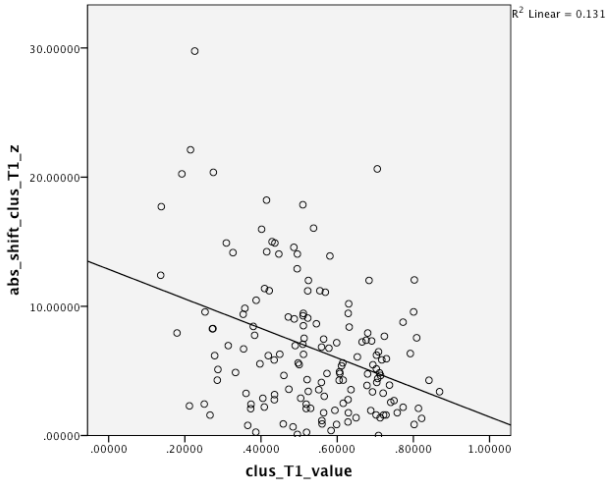

Figure 2.11 (c)

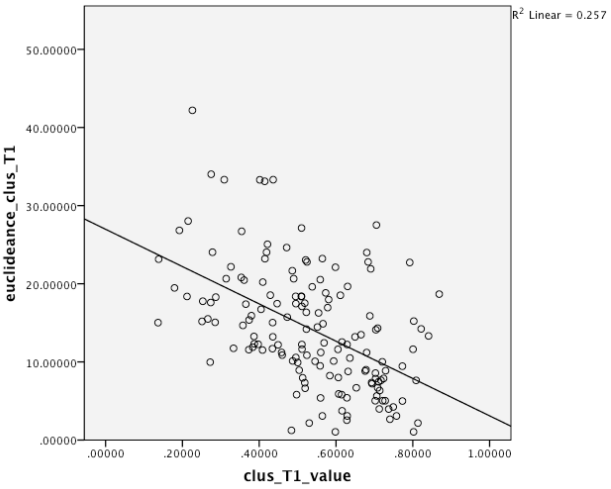

Figure 2.11 (d)

Figure 2.11 (a) Scatter plot of peak intensity versus absolute x distance away from ideal peak
(b) Scatter plot of peak intensity versus absolute y distance away from ideal peak
(c) scatter plot of peak intensity versus absolute z distance away from ideal peak
(d) scatter plot of peak intensity versus Euclidean distance away from ideal peak

As shown in Figure 2.11, the larger the shift away from the ideal point (irrespective of the direction) corresponds to a lower intensity of the peak vertex on the lesion side. This could be a confound suggesting increased noise in patients with larger deficits, seen as higher variability in peak location

and lower connectivity strength. To control for this we matched a motor deficit and no deficit group with similar peak intensities. This resulted in a motor deficit group (N = 28) with a average peak intensity of 0.54 and a no motor deficit group (N = 33) with a mean peak intensity of 0.58. This does not change the results, and there is still a trend of significance along X axis in medial direction ($df = 59$, $p = 0.058$). Furthermore, a significant absolute shift in the X direction ($df = 59$, $p < 0.001$), a trend in Y ($df = 59$, $p = 0.088$) and Z axis ($df = 59$, $p = 0.081$) directions and a significant Euclidean distance shift ($df = 59$, $p < 0.001$) showed up. To summarize, by removing the effect of intensity we validated that the shifting peak does not reflect the noise. This result further confirms that 2 weeks after stroke, the hand region tends to shift within varied directions, but most strongly along the medio-lateral axis.

2.3.2 Chronic stage and recovery

As mentioned before, we measured data including fMRI and behavior for stroke patients at three time-points: approximately two weeks after stroke (acute), three months after stroke (chronic 1) and one year after stroke (chronic 2). For the longitudinal analysis we separated our stroke patients into two groups based on their acute arm score (patients with lesion in the hand area are excluded): motor deficit group (N = 38) and no deficit group (N = 27). We similarly collected data at two time points (time point 1 and time point 2 with an interval of three months) for healthy subjects.

As for the sub-acute analysis, we created central sulcus correlation maps for each subject at each time-point (Figure 2.5 (b)). Then to investigate the similarity in the topography of correlation between acute and chronic, we computed the spatial correlation for each group (healthy subjects, motor deficit stroke patients and no deficit stroke patients) at each time-point using the time point 1 healthy subjects as an reference(Figure 2.12).

Figure 2.12 (a) time point 1 (b) time point 2

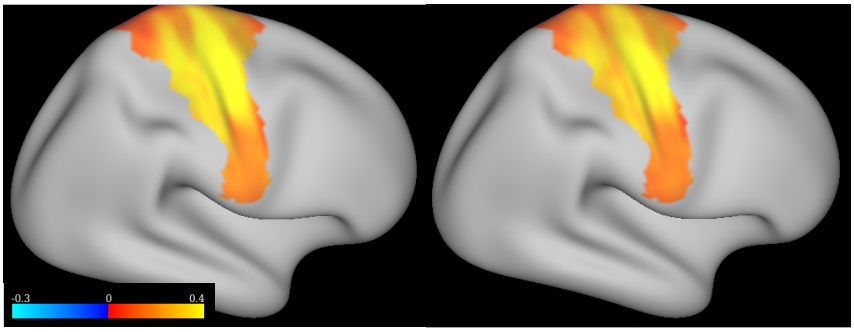

Figure 2.12 (a)(b) Average masked correlation maps for healthy subjects group

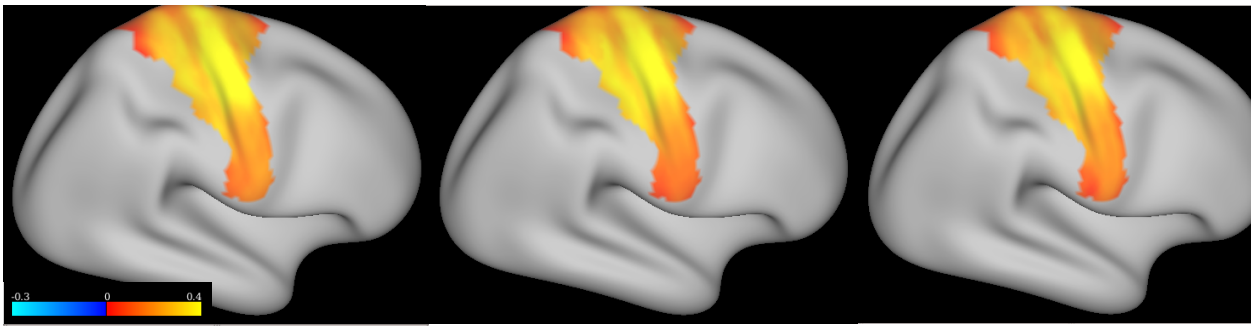

Figure 2.12 (c) acute **(d) chronic 1** **(e) chronic 2**

Figure 2.12 (c)(d)(e) Average masked correlation maps for the no deficit group

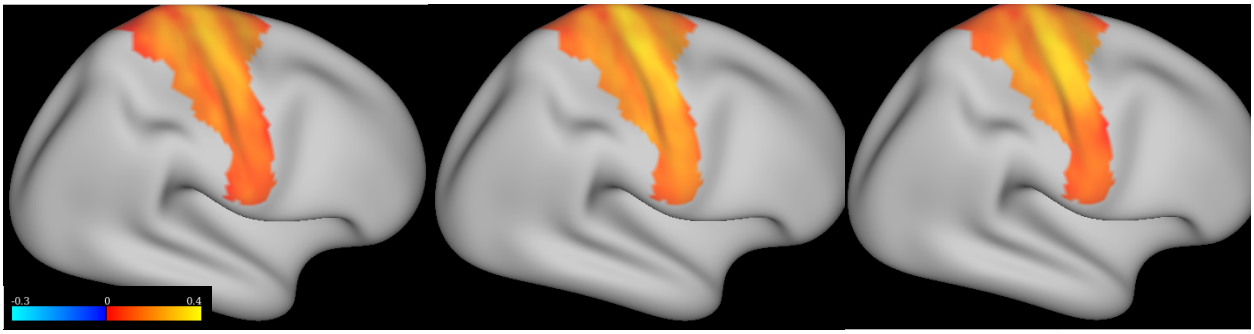

Figure 2.12 (f) acute **(g) chronic 1** **(h) chronic 2**

Figure 2.12 (f)(g)(h) Average masked correlation maps for motor deficit group

The average correlation maps for healthy subjects at two time points exhibit an obvious similarity ($r = 0.9589$, $p < 0.001$) with a clear yellow (which means high correlation of a region with the hand knob region in the other hemisphere). When comparing the no motor deficit average correlation map with the same (first time point) mean healthy subjects map, the spatial correlations also very high and very similar for each of the three time points (time-point 1: $r = 0.9323$, $p < 0.001$; time-

point 2: r = 0.9247, p < 0.001; time-point 3: r = 0.9048, r < 0.001). This indicates that stroke patients without motor deficits and healthy controls have similar surface FC from the hand knob in one hemisphere to the other. By comparison, the average map of the motor deficit group tends to change across the three time points (as correlated with the healthy controls, time-point 1: r = 0.7912, p < 0.001; time-point 2: r = 0.8227, p < 0.001; time-point 3: r = 0.9137, r < 0.001). This indicates that stroke patients with motor deficits have a spatial topography in the pre/post central sulcus that is different from healthy and stroke controls, which normalizes over time. Furthermore, we ran t test at the chronic stage for the peak location of the motor deficit and no deficit groups. We did not see any significant difference on X (df = 63, p = 0.988), Y (df = 63, p = 0.997) and Z direction (df = 63, p = 0.476). However, when comparing the absolute shift from the ideal point for these two groups, a significant shown again along X axis (df = 63, p = 0.003) and Z axis (df = 63, p = 0.016), but no in Y axis (df = 63, p = 0.778).

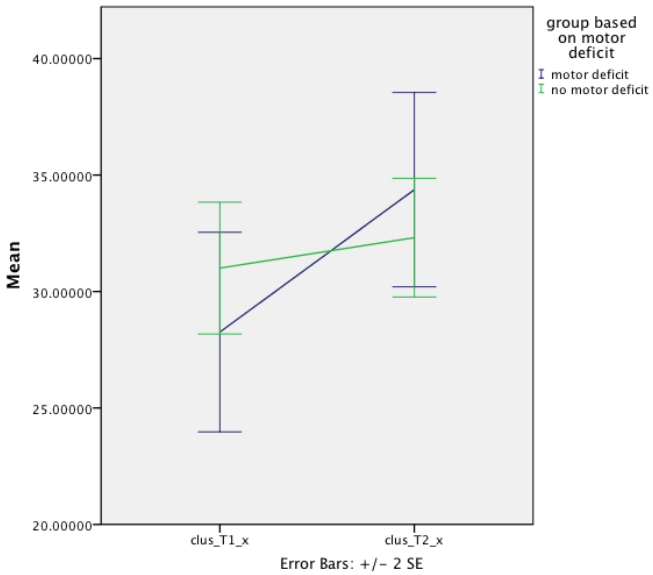

Figure 2.13 Mean of x coordinate at two time points of motor deficit and no deficit group

Since most recovery happens during the first three months post stroke, we chose to investigate the relationship of motor function recovery and the shift of the peak between 2 weeks and 3 months. We evaluated how the peaks shift over time (chronic - acute). By comparing the motor deficit group

and no motor deficit group with a repeated measures analysis of variance (ANOVA), we found a most obvious tendency of the peak shift along X coordinate in the motor deficit group moving towards the X location of no deficit group (Figure 2.13). Even though the interaction is not significant, the trend of a shift in the X direction from medial to lateral for the motor deficit subjects towards the no deficit group suggests a shift back towards a location more similar to normal.

To further investigate the shift during recovery, we wanted to relate the shifts to behavioral recovery. For each subject that had a motor deficit at the acute stage (N = 38), a recovery ratio taking into account both the initial score and the change score between the two time points: was calculated:

$$\boldsymbol{recovery\ ratio} = \frac{\boldsymbol{time\ 2\ arm\ score - time\ 1\ arm\ score}}{\boldsymbol{1 - time\ 1\ arm\ score}} \qquad (2.2)$$

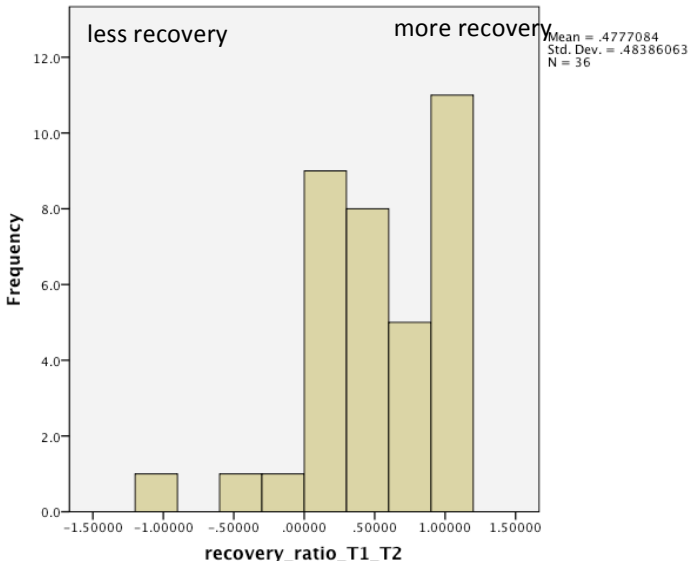

Figure 2.14 Recovery ratio summary from acute to chronic1

Figure 2.14 is the summary of recovery ratio of acute to chronic 1 for the motor deficit group subjects.

A score of 1 indicates full recovery, a score of 0 indicates no recovery, a negative score indicates worsening of motor functions. We ran a correlation between the recovery ratio and the absolute

value of shift from along the X, Y or Z axis or Euclidean distance at two time points. There was no significant correlation between the motor outcome and spatial shift along X axis ($r = 0.127$, $p = 0.461$), Y axis ($r = 0.212$, $p = 0.215$) and Z axis ($r = -0.168$, $p = 0.327$). However we can see a tendency of positive correlation along X axis in Figure 2.15. By checking the distribution of points in the figure, I think the reason that there is no significant relationship might be the very few subjects who recovery little during this time.

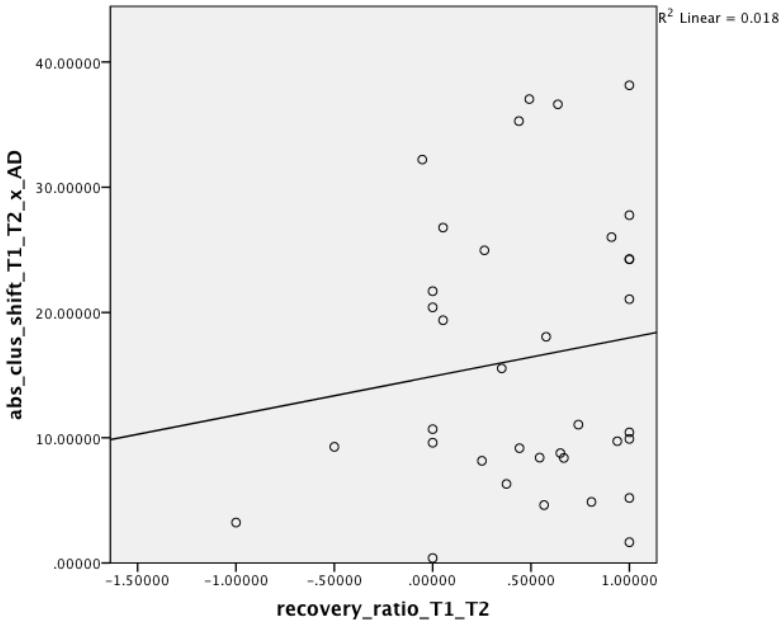

Figure 2.15 Scatter plot of recovery ratio versus absolute shift from acute to chronic along x axis

After investigating the shift longitudinally, we wanted to measure whether the intensity changed over time. The intensity of the region around peak vertex at all three time points for the motor deficit group and no deficit group (Figure 2.16) were investigated using region analysis.

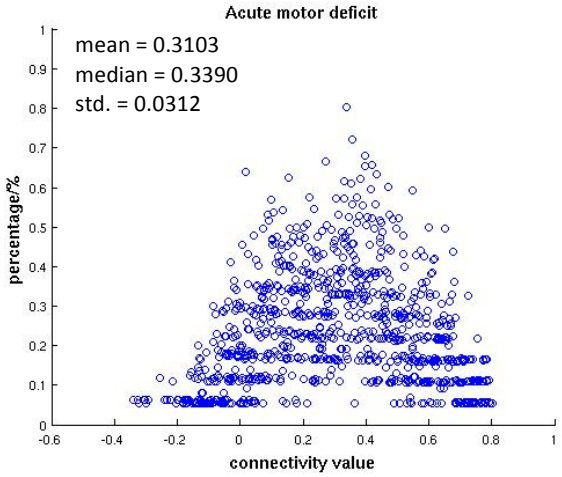

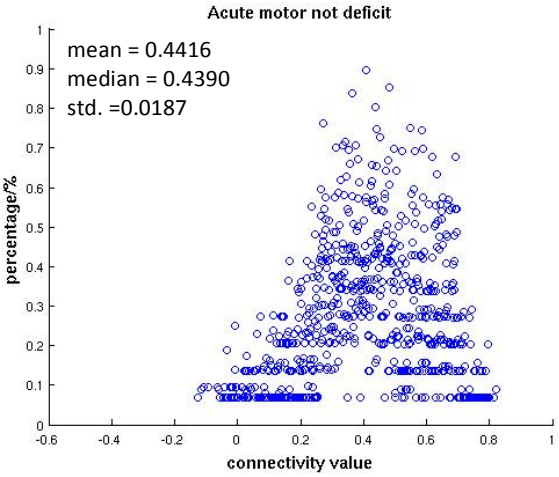

Figure 2.16 Acute stage: (a) motor deficit group **(b) the no deficit group**

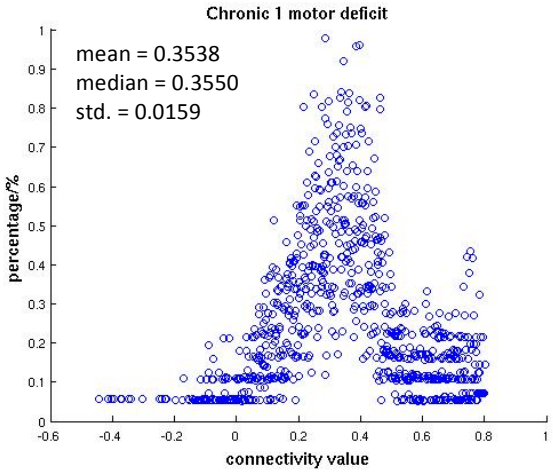

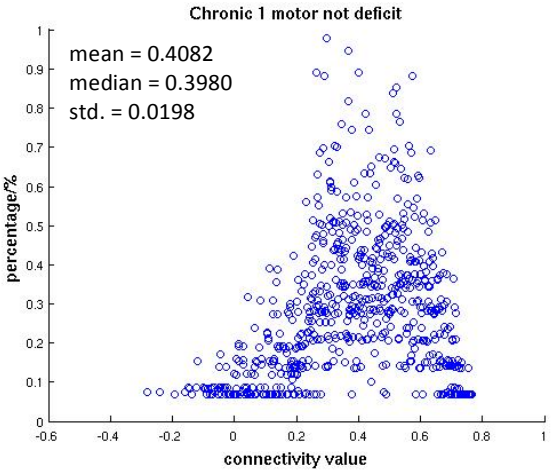

Figure 2.16 Chronic 1 stage: (c) motor deficit group **(d) the no deficit group**

We binned the correlation intensity data and applied fisher Z transformation (Silver and Dunlap 1987) to be able to compare the groups and time-points:

$$z = \frac{1}{2}\ln\left(\frac{1+r}{1-r}\right) \quad (2.3)$$

Where r is the initial correlation intensity and z is the transformed intensity. Then we ran a t-test based on the z transformed intensities between the motor deficit and no deficit groups as well as

within each of the groups over time. There is a significant difference between the groups at each time-point (acute: df = 10191, $p < 0.001$; chronic: df = 11617, $p < 0.001$), with a higher mean intensity for the no deficit group. This supports our hypothesis that the inter-hemisphere functional connection intensity in the hand area of lesioned hemisphere presents a decrease for the stroke patients with motor deficits. Within the no deficit group there was no change (from acute to chronic 1: df = 9351, $p = 0.1884$), whereas the deficit group, shows significant differences from acute to chronic 1 (df = 12457, $p < 0.001$) with an increase of mean intensity and decrease of standard deviation. This shows that during the first three months after stroke, patients with motor deficits at the acute stage exhibit recovery, seen as the increase of connection intensity with the hand area of the damaged hemisphere.

2.4 Discussion

In this study, we used the hand representation in the human primary motor cortex as the seed region of interest (ROI) and we evaluate its FC to/from other regions in the pre-central/post-central region of the contralateral hemisphere. In all analyses the target region is in the damaged hemisphere. We examined peak location and intensity as well as the topography over the whole region as computed by spatial correlation on ROI-to-surface maps, both acutely and chronically.

At the acute stage, we found that stroke patients who presented with arm deficits show a shift of peak coordinates on the lesion side as compared to healthy subjects and stroke patients who do not have arm deficits. The increased variation of peak vertices' location is especially obvious along the X axis and Z axis consistent with a shift along the motor cortex. Furthermore, we found an increase in the absolute shift (i.e. the variability of the peak irrespective of location) along X, Y, Z axis and the Euclidean distance. The later measures also correlated with the ARAT score (X and Z axis are trending). These findings suggest that since the leg representation is the region located dorsally to the hand area along the primary motor cortex, the directional shift could indicate an acute

remapping onto leg representation. The increased variability is also consistent with shifts in the motor peak representation, and this also correlates with behavioral deficits.

These result agree with a TMS study using motor evoked potential (MEP) to map the corticomotor projection to the hand, which demonstrated a medial-lateral shift of the center of the map for subcortical ischemic stroke patients (Thickbroom et al. 2004). By taking the arm score into consideration, we also found a significant correlation between the Euclidean distance shift away from ideal peak and the motor outcome.

Furthermore, both the mean and standard deviation differences of the correlation intensity between the motor deficit and no deficit group show a clear decrease of inter-hemisphere functional connectivity for the stroke patients who have motor deficit at acute stage. This indicates that the ipsilesional connection site does not only shift in location, but also reduces its intensity. Since the peak intensity also correlates with its absolute shift in the brain, more shifts (in all directions) will lead to larger decrease of the functional connectivity on the lesion side. After removing the effect of intensity on spatial shift by matching the peak intensity of motor deficit group and no deficit group this result was still present. Thus both the shift of the peak and the functional connectivity intensity correlate with the motor outcome two weeks after stroke without interference.

During the recovery process, we evaluated changes in motor FC over time after stroke. The shift of the peak location trends towards a normalization of the location, especially along X direction (medio-lateral). This shift to normalization seems to have a positive relationship with the motor outcome (recovery ratio), but they do not significantly correlate with each other. There are two possibilities that can explain it. First, by checking the distribution of the recovery ratio of motor deficit patients in our database, most of them recover a lot in the first 3 months. Therefore, as very few patients recover a little, the shift results are highly biased gathering in the high recovery part, which makes it hard to have a reasonable correlation from non-recovery to fully recovery. Second, maybe at this point, the shift is not restricted in particular X, Y and Z directions. We might need to

find the actual direction for the subjects. In addition, since intensity around ipsilesional peak for motor deficit group is lower compared to no deficit group at all three time points, this result is accordance to decreased cortico-cortico connectivity on the lesion side of the well-recovered chronic subcortical stroke patients (Gerloff et al. 2006).

The shift direction at acute stage and during recovery mainly along X axis could be explained by different potential mechanisms. Two weeks post stroke when limited time has passed to compensate for the damage caused by lesion, medio-lateral shift suggests the disconnected cortex is taken over by its neighbors within primary motor cortex (mainly dorsal: leg representation), which can happen through unmasking of existing, previously inactive pathways by decreasing intracortical inhibition (Jacobs and Donoghue 1991)., The recruitment of pre-existing pathways is expressed as an obvious increase of mean intensity in the region around peak. After that within the first three months after stroke, the shift along medio-lateral axis tended to shift back to normal (more similar to the no deficit group). This could be supported through sprouting axons and the formation of new synapses that acutally reconnect the cortex to structural pathways that were still intact, could take up to a few months (Lee et al. 2000).

In the future work, a normally functioning region (such as in the occipital lobe) that is not affected by the lesion could be used as a control region to control for inter-subject noise and variation. Furthermore, it might be worthwhile to measure the regions around hand area. For example, finding landmarks for the face or leg representation as seeds to evaluate the cortico-cortico functional connectivity on the lesioned side. In this manner potential of the neighboring regions can be investigated to see how the change of affected hand area influences other representations and if there is an increased overlap between regions.

References

Ago, T, T Kitazono, H Ooboshi, J Takada, T Yoshiura, F Mihara, S Ibayashi, and M Iida. 2003. "Deterioration of Pre-Existing Hemiparesis Brought about by Subsequent Ipsilateral Lacunar Infarction." *Journal of Neurology, Neurosurgery, and Psychiatry* 74 (8): 1152–53. doi:10.1136/jnnp.74.8.1152.

Altamura, Claudia, Kahtya Torquati, Filippo Zappasodi, Antonio Ferretti, Vittorio Pizzella, Francesco Tibuzzi, Fabrizio Vernieri, et al. 2007. "fMRI-vs-MEG Evaluation of Post-Stroke Interhemispheric Asymmetries in Primary Sensorimotor Hand Areas." *Experimental Neurology* 204 (2): 631–39. doi:10.1016/j.expneurol.2006.12.017.

Anbeek, Petronella, Koen L. Vincken, Matthias J P Van Osch, Robertus H C Bisschops, and Jeroen Van Der Grond. 2004. "Probabilistic Segmentation of White Matter Lesions in MR Imaging." *NeuroImage* 21 (3): 1037–44. doi:10.1016/j.neuroimage.2003.10.012.

Ashburner, John, and Karl J. Friston. 2005. "Unified Segmentation." *NeuroImage* 26 (3): 839–51. doi:10.1016/j.neuroimage.2005.02.018.

Baldassarre, A, L E Ramsey, J Rengachary, K Zinn, J S Siegel, N V Metcalf, Strube M., A Z Snyder, and M Corbetta. 2016. "Dissociated Functional Connectivity Profiles for Motor and Attention Deficits in Acute Right-Hemisphere Stroke." *Brain*.

Baldassarre, Antonello, Lenny Ramsey, Carl L. Hacker, Alicia Callejas, Serguei V. Astafiev, Nicholas V. Metcalf, Kristi Zinn, et al. 2014. "Large-Scale Changes in Network Interactions as a Physiological Signature of Spatial Neglect." *Brain* 137 (12): 3267–83. doi:10.1093/brain/awu297.

Birgani, P.M., M. Ashtiyani, and S. Asadi. 2008. "MRI Segmentation Using Fuzzy C-Means Clustering Algorithm Basis Neural Network." *2008 3rd International Conference on Information and Communication Technologies: From Theory to Applications*. doi:10.1109/ICTTA.2008.4530110.

Black, Sandra, Fuqiang Gao, and Juan Bilbao. 2009. "Understanding White Matter Disease: Imaging-Pathological Correlations in Vascular Cognitive Impairment." *Stroke* 40 (3 SUPPL. 1): 48–53. doi:10.1161/STROKEAHA.108.537704.

Byrnes, Michelle L., Gary W. Thickbroom, Bev A. Phillips, and Frank L. Mastaglia. 2001. "Long-Term Changes in Motor Cortical Organisation after Recovery from Subcortical Stroke." *Brain Research* 889 (1-2): 278–87. doi:10.1016/S0006-8993(00)03089-4.

Calautti, Cinzia, Francois Leroy, Jean Yves Guincestre, and Jean Claude Baron. 2003. "Displacement of Primary Sensorimotor Cortex Activation after Subcortical Stroke: A Longitudinal PET Study with Clinical Correlation." *NeuroImage* 19 (4): 1650–54. doi:10.1016/S1053-8119(03)00205-2.

Carmichael, S. Thomas. 2006. "Cellular and Molecular Mechanisms of Neural Repair after Stroke: Making Waves." *Annals of Neurology* 59 (5): 735–42. doi:10.1002/ana.20845.

Carmichael, S. Thomas, Ivonne Archibeque, Linslee Luke, Tim Nolan, Janneth Momiy, and Songlin Li. 2005. "Growth-Associated Gene Expression after Stroke: Evidence for a Growth-

Promoting Region in Peri-Infarct Cortex." *Experimental Neurology* 193 (2): 291–311. doi:10.1016/j.expneurol.2005.01.004.
Carter, Alex R., Gordon L. Shulman, and Maurizio Corbetta. 2012. "Why Use a Connectivity-Based Approach to Study Stroke and Recovery of Function?" *NeuroImage* 62 (4). Elsevier Inc.: 2271–80. doi:10.1016/j.neuroimage.2012.02.070.
Chen, C L, F T Tang, H C Chen, C Y Chung, and M K Wong. 2000. "Brain Lesion Size and Location: Effects on Motor Recovery and Functional Outcome in Stroke Patients." *Archives of Physical Medicine and Rehabilitation* 81 (April): 447–52. doi:10.1053/mr.2000.3837.
Chen, R, L G Ã Cohen, and M Hallett. 2002. "Nervous System Reorganization Following Injury" 111 (4): 761–73.
Cohen, L G, P Celnik, A Pascual-Leone, B Corwell, L Falz, J Dambrosia, M Honda, et al. 1997. "Functional Relevance of Cross-Modal Plasticity in Blind Humans." *Nature* 389 (6647): 180–83. doi:10.1038/38278.
Corbetta, Maurizio, Lenny Ramsey, Alicia Callejas, Antonello Baldassarre, Carl D. Hacker, Joshua S. Siegel, Serguei V. Astafiev, et al. 2015. "Common Behavioral Clusters and Subcortical Anatomy in Stroke." *Neuron* 85 (5). Elsevier Inc.: 927–41. doi:10.1016/j.neuron.2015.02.027.
Cramer, Steven C., and Kit R. Crafton. 2006. "Somatotopy and Movement Representation Sites Following Cortical Stroke." *Experimental Brain Research* 168 (1-2): 25–32. doi:10.1007/s00221-005-0082-2.
Dice, Lee R. 1945. "Measures Of The Amount Of Ecologic Association Between Species." *Ecology* 26 (3): 297–302.
Dijkhuizen, R M, J Ren, J B Mandeville, O Wu, F M Ozdag, M A Moskowitz, B R Rosen, and S P Finklestein. 2001. "Functional Magnetic Resonance Imaging of Reorganization in Rat Brain after Stroke." *Proc Natl Acad Sci U S A* 98 (22): 12766–71. doi:10.1073/pnas.231235598\r231235598 [pii].
Donoghue, J P, G Hess, and J N Sanes. 1996. "Substrates and Mechanisms for Learning in Motor Cortex." *Acquisition of Motor Behavior in Vertebrates*. MIT Press Cambridge, MA, 363–86.
Donoghue, J P, and J N Sanes. 1987. "Peripheral Nerve Injury in Developing Rats Reorganizes Representation Pattern in Motor Cortex." *Proceedings of the National Academy of Sciences of the United States of America* 84 (4): 1123–26. doi:10.1073/pnas.84.4.1123.
Drury, H a, D C Van Essen, C H Anderson, C W Lee, T a Coogan, and J W Lewis. 1996. "Computerized Mappings of the Cerebral Cortex: A Multiresolution Flattening Method and a Surface-Based Coordinate System." *Journal of Cognitive Neuroscience* 8 (1): 1–28. doi:10.1162/jocn.1996.8.1.1.
Elbert, Thomas, and Brigitte Rockstroh. 2004. "Reorganization of Human Cerebral Cortex: The Range of Changes Following Use and Injury." *The Neuroscientist : A Review Journal Bringing Neurobiology, Neurology and Psychiatry* 10 (2): 129–41. doi:10.1177/1073858403262111.
Feng, Dai, Luke Tierney, and Vincent Magnotta. 2012. "MRI Tissue Classification Using High-Resolution Bayesian Hidden Markov Normal Mixture Models." *Journal of the American Statistical Association* 107 (497): 102–19. doi:10.1198/jasa.2011.ap09529.
Filley, Christopher M. 2012. "White Matter Dementia." *Therapeutic Advances in Neurological Disorders* 5

(5): 267–77. doi:10.1177/1756285612454323.
Fischl, B, M I Sereno, and A M Dale. 1999. "Cortical Surface-Based Analysis II: Inflation, Flattening, and a Surface-Based Coordinate System." *NeuroImage* 9 (2): 195–207. doi:10.1006/nimg.1998.0396.
Fischl, Bruce, Martin I. Sereno, Roger B H Tootell, and Anders M. Dale. 1999. "High-Resolution Intersubject Averaging and a Coordinate System for the Cortical Surface." *Human Brain Mapping* 8 (4): 272–84. doi:10.1002/(SICI)1097-0193(1999)8:4<272::AID-HBM10>3.0.CO;2-4.
Fisher, C M. 1992. "Concerning the Mechanism of Recovery in Stroke Hemiplegia." *Can J Neurol Sci* 19 (1): 57–63. http://www.ncbi.nlm.nih.gov/entrez/query.fcgi?cmd=Retrieve&db=PubMed&dopt=Citation&list_uids=1562908.
Florence, Sherre L., Hilary B. Taub, Kaas Jon H., and Jon H. Kaas. 1998. "Large-Scale Sprouting of Cortical Connections after Peripheral Injury in Adult Macaque Monkeys." *Science* 282 (November): 1117–21. doi:10.1126/science.282.5391.1117.
García-Lorenzo, Daniel, Simon Francis, Sridar Narayanan, Douglas L. Arnold, and D. Louis Collins. 2013. "Review of Automatic Segmentation Methods of Multiple Sclerosis White Matter Lesions on Conventional Magnetic Resonance Imaging." *Medical Image Analysis* 17 (1): 1–18. doi:10.1016/j.media.2012.09.004.
Gerloff, Christian, Khalaf Bushara, Alexandra Sailer, Eric M. Wassermann, Robert Chen, Takahiro Matsuoka, Daniel Waldvogel, et al. 2006. "Multimodal Imaging of Brain Reorganization in Motor Areas of the Contralesional Hemisphere of Well Recovered Patients after Capsular Stroke." *Brain* 129 (3): 791–808. doi:10.1093/brain/awh713.
Glasser, Matthew F., Stamatios N. Sotiropoulos, J. Anthony Wilson, Timothy S. Coalson, Bruce Fischl, Jesper L. Andersson, Junqian Xu, et al. 2013. "The Minimal Preprocessing Pipelines for the Human Connectome Project." *NeuroImage* 80. Elsevier Inc.: 105–24. doi:10.1016/j.neuroimage.2013.04.127.
Gordon, E. M., T. O. Laumann, B. Adeyemo, J. F. Huckins, W. M. Kelley, and S. E. Petersen. 2014. "Generation and Evaluation of a Cortical Area Parcellation from Resting-State Correlations." *Cerebral Cortex*, bhu239 – . doi:10.1093/cercor/bhu239.
Green, J B, E Sora, Y Bialy, a Ricamato, and R W Thatcher. 1998. "Cortical Sensorimotor Reorganization after Spinal Cord Injury: An Electroencephalographic Study." *Neurology* 50 (4): 1115–21. doi:10.1212/WNL.50.4.1115.
Grefkes, Christian, and Gereon R. Fink. 2011. "Reorganization of Cerebral Networks after Stroke: New Insights from Neuroimaging with Connectivity Approaches." *Brain* 134 (5): 1264–76. doi:10.1093/brain/awr033.
Greicius, Michael D., Kaustubh Supekar, Vinod Menon, and Robert F. Dougherty. 2009. "Resting-State Functional Connectivity Reflects Structural Connectivity in the Default Mode Network." *Cerebral Cortex* 19 (1): 72–78. doi:10.1093/cercor/bhn059.
Hanson, Lars G. 2008. "Is Quantum Mechanics Necessary for Understanding Magnetic Resonance?" *Concepts in Magnetic Resonance Part A: Bridging Education and Research* 32 (5): 329–40. doi:10.1002/cmr.a.20123.
Hornak, Joseph P. 2008. "The Basics of MRI, 2008." *URL Http://www. Cis. Rit.*

Edu/htbooks/mri/index. Html 68.
Hubel, D H, and T N Wiesel. 1970. "The Period of Susceptibility to the Physiological Effects of Unilateral Eye Closure in Kittens." *J. Physiol.* 206: 419–36.
Jacobs, Kimberle M., and John P. Donoghue. 1991. "Reshaping the Cortical Motor Map by Unmasking Latent Intracortical Connections." *Science* 251 (4996): 944–47.
Jang, Sung Ho, Kyoung Kim, Seong Ho Kim, Su Min Son, Woo Hyuk Jang, and Hyeok Gyu Kwon. 2014. "The Relation between Motor Function of Stroke Patients and Diffusion Tensor Imaging Findings for the Corticospinal Tract." *Neuroscience Letters* 572. Elsevier Ireland Ltd: 1–6. doi:10.1016/j.neulet.2014.04.044.
Kaas, Jon H, and Hui-Xin Qi. 2004. "The Reorganization of the Motor System in Primates after the Loss of a Limb." *Restorative Neurology and Neuroscience* 22 (3-5): 145–52. http://www.ncbi.nlm.nih.gov/pubmed/15502261.
Kaas, Jon H. 2000. "The Reorganization of Somatosensory and Motor Cortex after Peripheral Nerve or Spinal Cord Injury in Primates." *Progress in Brain Research* 128: 173–79. doi:10.1016/S0079-6123(00)28015-1.
Kim, Seong-Gi, and Seiji Ogawa. 2012. "Biophysical and Physiological Origins of Blood Oxygenation Level-Dependent fMRI Signals." *Journal of Cerebral Blood Flow & Metabolism* 32 (7). Nature Publishing Group: 1188–1206. doi:10.1038/jcbfm.2012.23.
Koenig, S. H., R. D. Brown, M. Spiller, and N. Lundbom. 1990. "Relaxometry of Brain: Why White Matter Appears Bright in MRI." *Magnetic Resonance in Medicine* 14 (3): 482–95. doi:10.1002/mrm.1910140306.
Kwan, L T, B R Reed, J L Eberling, N Schuff, J Tanabe, D Norman, M W Weiner, and W J Jagust. 1999. "Effects of Subcortical Cerebral Infarction on Cortical Glucose Metabolism and Cognitive Function." *Archives of Neurology* 56 (7): 809–14. doi:10.1001/archneur.56.7.809.
Lao, Zhiqiang, Dinggang Shen, Dengfeng Liu, Abbas F. Jawad, Elias R. Melhem, Lenore J. Launer, R. Nick Bryan, and Christos Davatzikos. 2008. "Computer-Assisted Segmentation of White Matter Lesions in 3D MR Images Using Support Vector Machine." *Academic Radiology* 15 (3): 300–313. doi:10.1016/j.acra.2007.10.012.
Lee, M, H Reddy, S Pendlebury, M Jenkinson, S Smith, J Palace, and P M Matthews. 2000. "The Motor Cortex Shows Adaptive Functional Changes to Brain Injury from Multiple Sclerosis." *Annals of Neurology* 47: 606–13.
Maier, Oskar, Matthias Wilms, Janina von der Gablentz, Ulrike Krämer, and Heinz Handels. 2014. "Ischemic Stroke Lesion Segmentation in Multi-Spectral MR Images with Support Vector Machine Classifiers." *SPIE Medical Imaging* 9035: 903504. doi:10.1117/12.2043494.
Maier, Oskar, Matthias Wilms, Janina von der Gablentz, Ulrike M. Kramer, Thomas F. Munte, and Heinz Handels. 2015. "Extra Tree Forests for Sub-Acute Ischemic Stroke Lesion Segmentation in MR Sequences." *Journal of Neuroscience Methods* 240. Elsevier B.V.: 89–100. doi:10.1016/j.jneumeth.2014.11.011.
Marcus, Daniel S, John Harwell, Timothy Olsen, Michael Hodge, and Matthew F. Glasser. 2011. "Informatics and Data Mining Tools and Strategies for the Human Connectome Project." *Frontiers in Neuroinformatics* 5 (4): 1–12. papers3://publication/doi/10.3389/fninf.2011.00004/abstract.

Misaki, Masaya, Jonathan Savitz, Vadim Zotev, Raquel Phillips, Han Yuan, Kymberly D. Young, Wayne C. Drevets, and Jerzy Bodurka. 2015. "Contrast Enhancement by Combining T1- and T2-Weighted Structural Brain MR Images." *Magnetic Resonance in Medicine* 00: 1–12. doi:10.1002/mrm.25560.

Missir, O, C Dutheil-Desclercs, J F Meder, A Musolino, and D Fredy. 1988. "Central Sulcus Patterns at MRI." *Journal of Neuroradiology. Journal de Neuroradiologie* 16 (2): 133–44.

Murphy, Timothy H, and Dale Corbett. 2009. "Plasticity during Stroke Recovery: From Synapse to Behaviour." *Nature Reviews. Neuroscience* 10 (12). Nature Publishing Group: 861–72. doi:10.1038/nrn2735.

Navarro, X., Meritxell Vivó, and Antoni Valero-Cabré. 2007. "Neural Plasticity after Peripheral Nerve Injury and Regeneration." *Progress in Neurobiology* 82 (4): 163–201. doi:10.1016/j.pneurobio.2007.06.005.

Nudo, R J, and G W Milliken. 1996. "Reorganization of Movement Representations in Primary Motor Cortex Following Focal Ischemic Infarcts in Adult Squirrel Monkeys." *Journal of Neurophysiology* 75 (5): 2144–49. doi:8551360.

Nudo, Randolph J. 2006. "Mechanisms for Recovery of Motor Function Following Cortical Damage." *Current Opinion in Neurobiology* 16 (6): 638–44. doi:10.1016/j.conb.2006.10.004.

Ozenne, Brice, Fabien Subtil, Leif Stergaard, and Delphine Maucort-Boulch. 2014. "Spatially Regularized Mixture Model for Lesion Segmentation with Application to Stroke Patients." *Biostatistics* 16 (3): 580–95. doi:10.1093/biostatistics/kxv004.

Pascual-Leone, A, A Amedi, F Fregni, and L Merabet. 2005. "The Plastic Human Brain Cortex." *Annual Review of Neuroscience* 28 (1): 377–401. doi:10.1146/annurev.neuro.27.070203.144216.

Pham, Dzung L., and Jerry L. Prince. 1999. "Adaptive Fuzzy Segmentation of Magnetic Resonance Images." *IEEE Transactions on Medical Imaging* 18 (9): 737–52. doi:10.1109/42.802752.

Pineiro, R, S Pendlebury, Heidi Johansen-Berg, and P M Matthews. 2001. "Functional MRI Detects Posterior Shifts in Primary Sensorimotor Cortex Activation after Stroke: Evidence of Local Adaptive Reorganization?" *Stroke; a Journal of Cerebral Circulation* 32 (5): 1134–39. doi:10.1161/01.STR.32.5.1134.

Rademacher, J., V. S. Caviness, H. Steinmetz, and a. M. Galaburda. 1993. "Topographical Variation of the Human Primary Cortices: Implications for Neuroimaging, Brain Mapping, and Neurobiology." *Cerebral Cortex* 3 (4): 313–29. doi:10.1093/cercor/3.4.313.

Robb, Richard Arlin, and Dennis P Hanson. 1991. "A Software System for Interactive and Quantitative Visualization of Multidimensional Biomedical Images." *Australasian Physical & Engineering Sciences in Medicine/supported by the Australasian College of Physical Scientists in Medicine and the Australasian Association of Physical Sciences in Medicine* 14 (1): 9–30.

Rowland, Douglas J., Joel R. Garbow, Richard Laforest, and Abraham Z. Snyder. 2005. "Registration of [18F]FDG microPET and Small-Animal MRI." *Nuclear Medicine and Biology* 32 (6): 567–72. doi:10.1016/j.nucmedbio.2005.05.002.

Schmidt, Mark, Ilya Levner, Russell Greiner, Albert Murtha, and Aalo Bistritz. 2005. "Segmenting Brain Tumors Using Alignment-Based Features." *Proceedings - ICMLA 2005: Fourth International Conference on Machine Learning and Applications* 2005: 218–20. doi:10.1109/ICMLA.2005.56.

Schwartz, E.L., A. Shaw, and E. Wolfson. 1989. "A Numerical Solution to the Generalized

Mapmaker's Problem:\nflattening Nonconvex Polyhedral Surfaces." *Pattern Analysis and Machine Intelligence, IEEE Transactions on* 11 (9): 1005–8. doi:10.1109/34.35506.
Seghier, Mohamed L., Karl J. Friston, and Cathy J. Price. 2007. "Detecting Subject-Specific Activations Using Fuzzy Clustering." *NeuroImage* 36 (3). Elsevier Inc.: 594–605. doi:10.1016/j.neuroimage.2007.03.021.
Seghier, Mohamed L., Anil Ramlackhansingh, Jenny Crinion, Alexander P. Leff, and Cathy J. Price. 2008. "Lesion Identification Using Unified Segmentation-Normalisation Models and Fuzzy Clustering." *NeuroImage* 41 (4): 1253–66. doi:10.1016/j.neuroimage.2008.03.028.
Selemon, Lynn D, Grazyna Rajkowska, and Patricia S Goldman-Rakic. 1995. "Abnormally High Neuronal Density in the Schizophrenic Cortex: A Morphometric Analysis of Prefrontal Area 9 and Occipital Area 17." *Archives of General Psychiatry* 52 (10). American Medical Association: 805–18.
Shi, Lin, Defeng Wang, Shangping Liu, Yuehua Pu, Yilong Wang, Winnie C W Chu, Anil T. Ahuja, and Yongjun Wang. 2013. "Automated Quantification of White Matter Lesion in Magnetic Resonance Imaging of Patients with Acute Infarction." *Journal of Neuroscience Methods* 213 (1). Elsevier B.V.: 138–46. doi:10.1016/j.jneumeth.2012.12.014.
Silver, N Clayton, and William P Dunlap. 1987. "Averaging Correlation Coefficients: Should Fisher's Z Transformation Be Used?" *Journal of Applied Psychology* 72 (1). American Psychological Association: 146.
Stamatakis, Emmanuel A., and Lorraine K. Tyler. 2005. "Identifying Lesions on Structural Brain Images - Validation of the Method and Application to Neuropsychological Patients." *Brain and Language* 94 (2): 167–77. doi:10.1016/j.bandl.2004.12.010.
Stensaas, Suzanne S, Donald K Eddington, and William H Dobelle. 1974. "The Topography and Variability of the Primary Visual Cortex in Man." *Neurosurg.* 40: 747–55.
Swets, John A, Ronald M Pickett, Susan F Whi, David J Getty, James A Schnur, Joel B Swets, and Barbara A Fi. 1979. "Assessment of Diagnostic Technologies." *Science* 205 (4407): 753–59. doi:10.1126/science.462188.
Talairach, J, and P Tournoux. 1988. *Co-Planar Stereotaxic Atlas of the Human Brain. 3-Dimensional Proportional System: An Approach to Cerebral Imaging*. New York: Thieme. citeulike-article-id:745727.
Thickbroom, Gary W., Michelle L. Byrnes, Sarah A. Archer, and Frank L. Mastaglia. 2004. "Motor Outcome after Subcortical Stroke Correlates with the Degree of Cortical Reorganization." *Clinical Neurophysiology* 115 (9): 2144–50. doi:10.1016/j.clinph.2004.04.001.
Thompson, P M, C Schwartz, R T Lin, a a Khan, and a W Toga. 1996. "Three-Dimensional Statistical Analysis of Sulcal Variability in the Human Brain." *The Journal of Neuroscience : The Official Journal of the Society for Neuroscience* 16 (13): 4261–74. http://www.ncbi.nlm.nih.gov/pubmed/8753887.
Tu, Zhuowen, Xiangrong Chen, Alan L Yuille, and Monte Carlo. 2005. "Image Parsing : Unifying Segmentation , Detection , and Recognition" 63 (2): 113–40.
Van Den Heuvel, Martijn P., and Hilleke E Hulshoff Pol. 2010. "Specific Somatotopic Organization of Functional Connections of the Primary Motor Network during Resting State." *Human Brain*

Mapping 31 (4): 631–44. doi:10.1002/hbm.20893.
Van Essen, David C., Heather a. Drury, James Dickson, John Harwell, Donna Hanlon, and Charles H. Anderson. 2001. "An Integrated Software Suite for Surface-Based Analyses of Cerebral Cortex." *Journal of the American Medical Informatics Association* 8 (5): 443–59. doi:10.1136/jamia.2001.0080443.
Volz, Lukas J, Anna-Sophia Sarfeld, Svenja Diekhoff, Anne K Rehme, Eva-Maria Pool, Simon B Eickhoff, Gereon R Fink, and Christian Grefkes. 2014. "Motor Cortex Excitability and Connectivity in Chronic Stroke: A Multimodal Model of Functional Reorganization." *Brain Structure & Function*, 1093–1107. doi:10.1007/s00429-013-0702-8.
Waldvogel, Daniel, Peter van Gelderen, Kenji Ishii, and Mark Hallett. 1999. "The Effect of Movement Amplitude on Activation in Functional Magnetic Resonance Imaging Studies." *Journal of Cerebral Blood Flow & Metabolism* 19 (11). Nature Publishing Group: 1209–12.
Wandell, B a, S Chial, and B T Backus. 2000. "Visualization and Measurement of the Cortical Surface." *Journal of Cognitive Neuroscience* 12 (5): 739–52. doi:10.1162/089892900562561.
Wang, Rui, Chao Li, Jie Wang, Xiaoer Wei, Yuehua Li, Chun Hui, Yuemin Zhu, and Su Zhang. 2014. "Automatic Segmentation of White Matter Lesions on Magnetic Resonance Images of the Brain by Using an Outlier Detection Strategy." *Magnetic Resonance Imaging* 32 (10). Elsevier Inc.: 1321–29. doi:10.1016/j.mri.2014.08.010.
Wieloch, Tadeusz, and Karoly Nikolich. 2006. "Mechanisms of Neural Plasticity Following Brain Injury." *Current Opinion in Neurobiology* 16 (3): 258–64. doi:10.1016/j.conb.2006.05.011.
Wilson, D a, R M Sullivan, and M Leon. 1987. "Single-Unit Analysis of Postnatal Olfactory Learning: Modified Olfactory Bulb Output Response Patterns to Learned Attractive Odors." *The Journal of Neuroscience : The Official Journal of the Society for Neuroscience* 7 (10): 3154–62.
Yousry, T. A., U. D. Schmid, H. Alkadhi, D. Schmidt, A. Peraud, A. Buettner, and P. Winkler. 1997. "Localization of the Motor Hand Area to a Knob on the Precentral Gyrus. A New Landmark." *Brain* 120 (1): 141–57. doi:10.1093/brain/120.1.141.